Serial stimulation of invariant natural killer T cells with covalently stabilized bispecific T cell engagers generates anti-tumor immunity while avoiding anergy

Kharkwal, Shalu Sharma; Johndrow, Christopher T; Veerapen, Natacha; Kharkwal, Himanshu; Saavedra-Avila, Noemi A; Carreño, Leandro J; Rothberg, Samantha; Zhang, Jinghang; Garforth, Scott J; Jervis, Peter J; Zhang, Lianjun; Donda, Alena; Besra, Amareeta K; Cox, Liam R; Almo, Steven C; Howell, Alan; Evans, Elizabeth E; Zauderer, Maurice; Besra, Gurdyal S; Porcelli, Steven A

Document Version
Peer reviewed version

Link to publication on Research at Birmingham portal

Title:

Serial Stimulation of Invariant Natural Killer T Cells with Covalently Stabilized Bispecific T Cell Engagers Generates Anti-Tumor Immunity While Avoiding Anergy

Authors:

Shalu Sharma Kharkwal[1,12], Christopher T. Johndrow[1], Natacha Veerapen[3], Himanshu Kharkwal[5,12], Noemi A. Saavedra-Avila[1], Leandro J. Carreño[1,6], Samantha Rothberg[1], Jinghang Zhang[1], Scott J. Garforth[2], Peter J. Jervis[7], Lianjun Zhang[8,9], Alena Donda[10], Amareeta K. Besra[3], Liam R. Cox[4], Steven C. Almo[2], Alan Howell[11], Elizabeth E. Evans[11], Maurice Zauderer[11], Gurdyal S. Besra[3], Steven A. Porcelli[1]*

Affiliations:

[1]Department of Microbiology and Immunology, and

[2]Department of Biochemistry, Albert Einstein College of Medicine, 1300 Morris Park Avenue, Bronx, NY 10461 2

[3]School of Biosciences, and [4]School of Chemistry, University of Birmingham, Edgbaston, Birmingham B15 2TT, UK.

[5]Department of Clinical Oncology, Montefiore Medical Centre, Eastchester Road, Bronx, NY 10461

[6]Millennium Institute on Immunology and Immunotherapy, ICBM, Facultad de Medicina, Universidad de Chile, Santiago 8380453, Chile

[7]Centre of Chemistry, University of Minho, Campus de Gualtar, 4710-057 Braga, Portugal

[8]Suzhou Institute of Systems Medicine, Suzhou, Jiangsu 215123, China

[9]Center for Systems Medicine, Institute of Basic Medical Sciences, Chinese Academy of Medical Sciences and Peking Union Medical College, 100005 Beijing, China;

[10]Department of Oncology and Ludwig Center for Cancer Research, University of Lausanne, Epalinges 1066, Switzerland

[11]Vaccinex Inc., Rochester, NY 14620

[12]Elstar Therapeutics, 840 Memorial Drive, Cambridge, MA 02139

Running Title:

Covalently stabilized BiTEs for activating iNKT cells

*Corresponding author:

Steven A. Porcelli, MD

Albert Einstein College of Medicine

Department of Microbiology and Immunology

1300 Morris Park Avenue

Tel: 718 430-3228

FAX: 718 430-8711

Email: steven.porcelli@einsteinmed.org

Abstract

CD1d-restricted invariant natural killer T cells (iNKT cells) mediate strong anti-tumor immunity when stimulated by glycolipid agonists. However, attempts to develop effective iNKT cell agonists for clinical applications have been thwarted by potential problems with dose-limiting toxicity and by activation-induced iNKT cell anergy, which limits the efficacy of repeated administration. To overcome these issues, we developed a unique bispecific T cell engager (BiTE) based on covalent conjugates of soluble CD1d with photoreactive analogs of the glycolipid α-galactosylceramide. Here we characterize the in vivo activities of iNKT cell-specific BiTEs and assess their efficacy for cancer immunotherapy in mouse models using transplantable colorectal cancer or melanoma tumor lines engineered to express human Her2 as a tumor-associated antigen. Systemic administration of conjugated BiTEs stimulated multiple iNKT cell effector functions including cytokine release, secondary activation of NK cells, and induction of dendritic cell maturation and also initiated epitope spreading for tumor-specific CD8+ cytolytic T cell responses. The anti-tumor effects of iNKT cell activation with conjugated BiTEs were further enhanced by simultaneous checkpoint blockade with antibodies to CTLA-4, providing a potential approach for combination immunotherapy. Multiple injections of covalently stabilized iNKT cell-specific BiTEs activated iNKT cells without causing iNKT anergy and exhaustion, thus enabling repeated administration for effective and nontoxic cancer immunotherapy regimens.

Statement of significance: Covalently stabilized conjugates that engage the antigen receptors of iNKT cells and target a tumor antigen activate potent anti-tumor immunity without induction of anergy or depletion of the responding iNKT cells.

4

Introduction

Invariant Natural Killer T (iNKT) cells are a conserved subset of specialized T cells that contribute to many innate and adaptive immune responses (1). Unlike conventional T cells, iNKT cells express T cell antigen receptors (TCRs) of limited diversity, and respond to specific foreign and self-glycolipid antigens presented by the MHC class I-like CD1d protein (2). The best characterized glycolipid antigens recognized by iNKT cells are synthetic forms of α-galactosylceramide (αGalCer), which activate their proliferation, cytokine production and cytotoxic functions (3). Activation of iNKT cells by αGalCer influences downstream immune responses through rapid cytokine release and a range of cell contact dependent signals. Detailed studies in mouse models show that this generates multifaceted immune responses that include Natural Killer (NK) cell activation, dendritic cell maturation, enhanced conventional T cell priming, antibody production and reversal of immunosuppressive effects from regulatory cells (4-6).

In mouse models, many structural analogues of αGalCer have strong anti-tumor activities (7), suggesting that iNKT cell directed therapies could be useful for cancer immunotherapy in humans (8, 9). Several phase I clinical trials with αGalCer have been done in patients with advanced cancers (10-12), but progress has been hampered by potential toxicities, off-target effects and lack of clear efficacy. These problems are due in part to the uptake and presentation of glycolipids by a variety of different types of antigen presenting cells, leading to complicated and unpredictable outcomes (4, 13). Furthermore, the development of long-term unresponsiveness (anergy) and depletion of iNKT cells by multiple exposures to αGalCer following injection into mice makes repeated administration ineffective (14, 15). Approaches to activating iNKT cells that

could circumvent these issues are needed to advance the development of effective cancer immunotherapies.

Previous studies showed that delivery of αGalCer in complex with soluble CD1d proteins targeted to the surface of tumor cells could more precisely focus iNKT cell responses and reduce adverse effects (16, 17). Such complexes, representing a type of bispecific T cell engager (BiTE) (18), showed improvements over free glycolipid in terms of sustained iNKT functionality and improved anti-tumor efficacy in these studies. However, the reversible glycolipid binding and rapid dissociation *in vivo* resulted in reduced functionality of iNKT cells, and other potential problems similar to those associated with free glycolipid (19). To overcome this limitation, we developed an approach for precise covalent conjugation of CD1d with αGalCer analogues containing a photoactivatable benzophenone group to create covalently stabilized iNKT cell specific activators (20). In the current study, we have extended our analysis of the immunological effects of iNKT cell activation by soluble tumor targeted, glycolipid conjugated iNKT cell specific BiTEs, and demonstrate their substantial anti-cancer effects in mouse models. Compared to free glycolipids or noncovalent complexes of CD1d with αGalCer, we found that covalently stabilized conjugates were significantly more effective at inducing iNKT activation, maturation of dendritic cells and secondary activation of NK cells and T cells, and did so without causing iNKT cell anergy following repeated administration. Target specificity was incorporated into conjugates by genetically fusing soluble CD1d with a single chain antibody domain with specificity for a tumor associated antigen, thus facilitating direct cytotoxic effects of iNKT cells and driving sustained immune responses within tumors to improve therapeutic outcomes.

Materials and Methods

Animal models

Female C57BL/6J (B6) mice were obtained at age 6-8 weeks from Jackson Laboratories (JAX) and maintained in specific pathogen-free conditions. CD1d knockout mice with deletions in the *Cd1d1/Cd1d2* loci on the B6 background (strain B6.129S6-Del(3Cd1d2-Cd1d1)1Sbp/J) were obtained from JAX (RRID: IMSR_JAX:008881), and C57BL/6 mice with a deletion of the *Traj18* gene (Jα18^{-/-} mice) were from Dr. Mitchell Kronenberg (La Jolla Institute for Allergy and Immunology). Human CD1d knock-in mice (B6.hCD1d-KI) were from Dr. Weiming Yuan (USC School of Medicine) (21). GFP expressing transgenic mice (strain C57BL/6-Tg(UBC-GFP)30Scha/J) were from JAX (RRID: IMSR_JAX:004353). All transgenic mice were bred in our facility. Female mice 10-12 weeks of age at the time of start of the experiments were used. All experiments requiring mice were conducted in compliance with institutional guidelines and under a protocol reviewed and approved by the Institutional Animal Care and Use Committee (IACUC) at Albert Einstein College of Medicine.

Glycolipid reagents

The iNKT cell α-GalCer glycolipid agonists C26:0 (KRN7000), C11:BP, 14C-labeled C11:BP and azido-C11:BP were synthesized and subsequently solubilized at 100 µM concentration in aqueous buffer (PBS + 0.1% DMSO + 0.05% Triton X-100) as described previously (13, 20).

CD1d tetramers and recombinant CD1d-ScFv fusion proteins

Murine single chain CD1d-β2m linked to AviTag™ and hexahistidine tags (MW ~57 kDa) was expressed and purified from stably transfected CHO cells as previously described (13, 22). Mouse CD1d tetramers were either prepared as described by Im et. al. (23) or obtained from the NIH Tetramer Core Facility (http://tetramer.yerkes.emory.edu/). Recombinant mouse or human CD1d fused to single chain antibody variable fragments (ScFv) against either huHER2 or human CEA were produced from transiently transfected HEK-293 cells as previously described (16, 17, 20). Glycolipid loading and covalent conjugation was performed as described previously (20) and in the supplemental methods.

Monoclonal antibodies, FACS and ELISA

Monoclonal antibody L363 (13, 24-26), was purified from supernatants of hybridoma cultures and biotinylated with EZ-Link™ Sulfo-NHS Biotinylation Kit (ThermoFisher). Effect of UV exposure on CD1d-C11:BP conjugate stability was determined by plate based dissociation assay (20). For FACS analyses, cells were stained with LIVE/DEAD™ Fixable Blue Dead Cell Stain Kit, for UV excitation (Thermo Fisher) or Zombie NIR™ Fixable Viability Kit (Biolegend). Fluorochrome conjugated mAb were obtained from commercial suppliers (Supplemental Table 1). Multiparameter FACS analyses incorporating up to 22 parameters were carried out using 5 laser LSRII (BD Biosciences) or 4 laser Aurora (Cytek) flow cytometers. All data analysis was done using FlowJo™ software (Becton Dickinson). Tumors were harvested aseptically for preparation of single cell suspensions. Methods for isolating tumor infiltrating lymphocytes are described in the supplemental materials. Tumor infiltrating iNKT cells

from all saline, complex or conjugate treated mice were gated as live, B220-, TCRβ+, αGalCer-loaded CD1d tetramer+ cells. For t-SNE analysis, 1500 total iNKT cells from each group were concatenated and run through 1000 iterations with perplexity of 30 and learning rate of 315. For serum cytokine ELISAs, capture antibodies were coated on wells of 96 well polystyrene microtiter plates (Supplemental Table 2), and wells were blocked using 5% BSA. Serum samples diluted 1:5 in PBS were added to allow binding of the cytokine of interest to the primary capture antibodies. Biotinylated secondary antibodies were then added, followed by washing and addition of Streptavidin-HRP. ELISAs were developed using Turbo-TMB substrate (Thermo Scientific) and read using a Wallac Victor plate reader. Data were analyzed using Prism 6.0 software (GraphPad). Hamster anti-CTLA-4 (Invivomab UC10-4F10, BioXcell) and purified normal hamster IgG (BioXcell) were used for *in vivo* CTLA4 blockade and isotype control respectively.

Cell lines

The murine colon carcinoma MC38 (RRID:CVCL_B288) and B16.F10 melanoma (RRID:CVCL_0159) tumor cell lines were obtained from the American Type Culture Collection (ATCC), and stable transfectants expressing huHER2 were produced as previously described (16). MC38 cells and transfectants were cultured in RPMI-1640 supplemented with 15% FBS. For transfectants, 1.2 µg/ml of puromycin was included in the medium. B16.F10 cells and transfectants were cultured in complete DMEM supplemented with 10% FBS, 10 mM HEPES, essential amino acids, glutamine and β-mercaptoethanol. For transfectants, 1.2 mg/ml Geneticin was added. Human iNKT clone HDD3 previously established from a random donor blood sample (27) was

maintained in complete RPMI-1640 medium containing 10% decomplemented human serum at 37°C in a humidified 5% CO_2 incubator. The cultures were expanded every 3-4 weeks by stimulation with phytohemagglutinin (PHA-P, Difco, Detroit, MI) in the presence of recombinant human IL-2 (250 IU/ mL; Chiron), recombinant human IL-7 (10 ng/mL; Peprotech) and irradiated (5000 Rad) allogeneic PBMCs. Cells were expanded by splitting cultures and feeding with fresh medium containing 250 IU/ml IL-2 and 10 ng/ml IL-7 every 2-3 days. Cell lines were maintained as frozen stocks at -150ºC and used in experiments within 2 weeks of thawing. Cell lines were not routinely tested for mycoplasma.

In vivo iNKT, NK and DC activation assays

Mice were injected i.v. with 0.4 nmoles (50 μg) of complexes or conjugates or an equimolar amount of free C11:BP or C26:0 (0.4 nmoles) in 0.1 ml of vehicle (PBS + 0.1% DMSO + 0.01% Tween-20). To quantitate cytokine secretion, mice were bled from the retro-orbital plexus at 2, 5, 10 and 24 hours and serum samples were prepared for quantitation of cytokines by capture ELISA. Kinetics of NK, iNKT and DC activation was determined in mice following i.v. injections of 0.4 nmoles of conjugates or complexes, or 0.4 nmoles of free glycolipid (αGalCer C26:0). Spleens were harvested at specific time points and splenocyte suspensions were stained as described in supplemental methods. NK and iNKT cells were stained for intracellular IFNγ. iNKT cells were quantitated as percentage of all live B220-, TCR-β low and CD1d tetramer+ cells. Tetramer+ iNKT cells were co-stained for relevant activation or inhibitory markers (CD69, CD28, NK1.1, ICOS, CTLA-4, LAG3, PD-1), and CD11c^{+} DC were co-stained

for activating or inhibitory ligands (CD80, CD86, PD-L1, PD-L2) and analyzed by flow cytometry. Assessment of iNKT cell anergy induction was done in mice primed by injection i.v. with 0.4 nmoles of complexes or conjugates (once, or three times at weekly intervals), or with saline or 0.4 nmoles of free glycolipid (αGalCer C26:0). Mice from all groups were restimulated with C26:0 on day 7 after the final priming dose, bled at 12 hours to quantitate serum IFNγ and sacrificed at 72 hours to determine iNKT numbers.

Tumor cell cytotoxicity assays

Direct cytotoxicity of tumor cells by iNKT cells was determined by standard ^{51}Cr release assay. Target cells (MC38-huHER2) labeled with 100 µCi ^{51}Cr as Na_2CrO_4 (Perkin Elmer) were co-cultured with human iNKT cell clone HDD3 at 1:1 E:T ratio for 12 hours at 37^0C, in the presence of anti-huHER2 complexes or conjugated BiTE (0.01- 10 µg/ml). Specific lysis was determined by measurement of gamma emmisions in the supernatant. For imaging of iNKT cell mediated tumor killing *in vitro*, MC38-huHER2 cells were seeded in 96 well Nunclon™ Sphera™ plates (ThermoFisher) at 3000 cells/well and grown for 5 days to allow formation of 3-dimensional tumor cell spheroids. Anti-huHER2 conjugated BiTEs or complexes containing either mouse or human CD1d were added to wells for a concentration of 10 µg/ml, and control wells received saline only. After incubating for 2 hours at 37ºC, unbound ligands were removed by centrifugation of plates and gentle washing with medium, followed by addition of 1000 purified mouse iNKT cells or 1000 human iNKT clone HDD3 cells in pre-warmed medium. Plates were then incubated for 12 hours before staining for apoptosis and necrosis using Apoptosos/Necrosis Assay Kit (Abcam) following the instructions

provided by the manufacturer. Confocal images of individual spheroids were acquired as Z-stacks with a Leica SP8 point scanning confocal microscope using a 10x air objective.

Mouse tumor immunotherapy models

Tumor cells harvested at mid-log phase were injected i.v. through the tail vein for the B16.F10-huHER2 melanoma model or grafted by subcutaneous injection into the thigh for the MC38-huHER2 carcinoma model. Immunotherapy agents were administered intravenously. Mice engrafted with B16.F10-huHER2 cells were sacrificed 16 days post injection Lungs were removed and digital photographs were obtained for calculation of the area of lung surface covered with melanized tumor using Image J software (RRID: SCR_003070) (https://imagej.nih.gov/ij/) (28). For animals grafted with subcutaneous MC38 cells, tumor volumes were measured on a daily basis using a digital caliper to obtain length and width. Tumor volume was calculated using the formula $V = (L \times W \times D) \times \pi/6$, as recommended in previous studies (29, 30). After attaining a tumor volume of approximately 1 cm^3, mice were monitored for up to two days, after which they were sacrificed if the tumor continued to grow as required by the approved animal research protocol. Mice were observed for up to 80 days, and animals lacking palpable tumors at the end of this period were considered complete responses.

To determine tumor antigen specific T cell responses in tumor bearing mice, IFNγ ELISPOT was performed on total T cells and CD8 depleted T cells purified from spleens. Tumor sections fixed in formalin were analyzed by histochemistry. To study distribution and kinetics of clearance of Conjugated BiTE, ^{14}C linked conjugates were

injected intravenously in tumor bearing mice. Mice were sacrificed at several time points to harvest organs. ^{14}C radioactivity was measured in CPM using liquid scintillation counter. Azide-linked conjugates were injected in mice to study tissue localization of conjugates. Frozen sections of harvested spleens, livers, kidneys and tumor were stained with DBCO-AF647 (31) and imaged using a panoramic slide scanner (3D Histek ltd.). For detailed methods see supplemental methods.

Statistical analysis

Results are shown as means ± 1 SE. Statistical significance between the groups was determined with 1-way or 2–way ANOVA test as indicated, and Sidak post-test was applied for data involving multiple comparisons. All P values were calculated using GraphPad Prism 6.0 software (RRID: SCR_002798). Values of $P < 0.05$ were considered significant.

Results

Activation of iNKT cells by covalent protein-glycolipid conjugates

Our previous work analyzed a series of photoactivable analogues of αGalCer containing a benzophenone (BP) moiety appended to a fatty acyl chain of varying length. An analogue containing an 11 carbon aliphatic chain (C11:BP, Fig. S1a) was optimal for iNKT cell stimulation when covalently conjugated to soluble mouse single chain CD1d-β2 microglobulin fusion proteins (mCD1d-β2m) by UV irradiation (20). For the current study, we produced BiTEs comprised of a mouse or human CD1d-β2m fusion proteins with single chain Fv (ScFv) antibody domains specific for the tumor associated antigen

HER2/neu linked to the C-termini (Supplementary Fig. 1b), as described previously (16, 20). The proteins were loaded with saturating amounts of glycolipids C11:BP or αGalCer C26:0 to prepare noncovalent protein-glycolipid complexes (Supplementary Fig. 1a). These were irradiated with UV light ($λ$ = 365 nm, dose of ~600 mJ/cm^2), activating the BP group in the case of C11:BP to form a covalent bond with the CD1d protein (20). Size exclusion chromatography showed the resulting conjugates to be predominantly monomeric (Supplementary Fig. 1b), and their covalent stabilization was validated by assessing residual binding of monoclonal antibody L363 (specific for CD1d containing a bound αGalCer ligand (24)) following mild detergent washing (Supplementary Fig. 1c).

Systemic administration of conjugated iNKT activators *in vivo* showed similar early activation of splenic iNKT cells for conjugates compared to the complexes and the benchmark of αGalCer injected as a free glycolipid, based on their levels of intracellular staining for IFNγ. Conjugates gave significantly stronger activation than an equivalent dose of complexes by this criterion, and responses to both complexes and conjugates were less sustained than the response to free αGalCer (Fig. 1a). A very similar pattern of response was observed for transactivation of NK cells, based on intracellular IFNγ levels in NK1.1$^+$ CD3 negative cells (Supplementary Fig. S2a-d). Mice lacking iNKT cells due to deletion of genes encoding either CD1d (Fig. 1b) or Jα18 (Supplementary Fig. S3a) showed no IFNγ secretion to either free glycolipid or conjugates, and adoptive transfer of purified iNKT cells into CD1d$^{-/-}$ mice restored responses to only conjugates but not to free αGalCer This confirmed that conjugates did not require CD1d expression by antigen presenting cells to stimulate *in vivo* responses.

Similar changes in levels of activation-inducible surface proteins on iNKT cells, including CD69, CD28, NK1.1 and ICOS, were observed following *in vivo* stimulation by complexes or conjugates (Fig. 1c). Sequential measurements of serum levels of IFNγ and other cytokines produced after iNKT cell activation, including IL-4, IL-12p70, TNFα (Fig. 1d), also showed rapid responses to complexes and conjugates, which were generally equivalent to or stronger than those stimulated by equimolar concentrations of free αGalCer C26:0. However, minimal iNKT cell expansion was observed following a single injection of complexes or conjugates, in contrast to the robust expansion at 72 hours followed by subsequent contraction of the splenic iNKT cells observed with a single injection of free αGalCer (Fig. 1e). Lack of expansion was further confirmed by selectively analyzing GFP⁺ iNKT cells that were adoptively transferred into wild type recipient mice prior to treatment with conjugates (Supplementary Fig. S3b). Thus, both complexes and conjugates stimulated a unique partial activation of iNKT cells *in vivo*, which was independent of normal antigen processing and presentation pathways requiring CD1d+ APCs. Such responses were characterized by strong transient cytokine production and faster NK transactivation, but without the proliferative expansion or subsequent contraction of iNKT cells normally associated with presentation of αGalCer (32, 33).

Reduced anergy with activation by conjugates

Induction of unresponsiveness (anergy) of iNKT cells after activation *in vivo* by free αGalCer is a major potential problem that limits the application of iNKT cell-directed therapies (14, 33, 34). To assess whether the partial activation observed with

complexes or conjugates also caused anergy, we analyzed responses to αGalCer in mice that had previously received complexes, conjugates or free αGalCer. As expected, the response to re-stimulation with αGalCer was markedly reduced in animals that had received a single prior injection of the glycolipid, based on serum IFNγ levels (Fig. 2a) and reduced iNKT cell expansion (Fig. 2b). Responses in animals that had previously received injections of complexes also showed evidence of anergy induction, with moderate reduction of IFNγ secretion and strong decreases in iNKT cell expansion. In contrast, a single injection of conjugates induced no evidence of anergy by these criteria, and three serial injections of conjugates gave only partial loss of expansion and no suppression of IFNγ secretion by iNKT cells. Despite the marked reduction in anergy, conjugates stimulated significant increases in surface expression of multiple inhibitory checkpoint receptors including CTLA-4, Lag3 and PD-1 by iNKT cells, especially in the liver (Fig. 2c), which may have contributed to the partial reduction in iNKT cell expansion associated with multiple conjugate injections. However, the expression of ligands for CTLA-4 and PD-1 on DCs was attenuated in conjugate treated versus free αGalCer treated animals (Fig. 2d), possibly mitigating the potential inhibitory effects of these receptors following multiple conjugate stimulations.

Enhanced anti-tumor activity of iNKT cell specific covalently stabilized BiTEs
Given the ability of conjugates to more strongly induce iNKT cell functions with less anergy than complexes, we directly compared iNKT cell specific BiTEs with and without covalent stabilization in mouse tumor immunotherapy models. For proof of concept studies, we incorporated the targeting capability of the anti-huHER2-specific ScFv fused

to murine CD1d. *In vitro* studies validated that the anti-huHER2 ScFv-mCD1d fusion

proteins bound specifically to tumor cells expressing huHER2, whereas similar fusion

proteins containing a ScFv domain specific for human CEA or a nonspecific control

ScFv did not bind detectably to huHER2 transfected cells (Supplementary Fig. S4a,b).

Initial studies to assess anti-tumor effects used a mouse metastatic melanoma cells

B16.F10 transfected to express huHER2. Following tumor cell injection, mice were

treated on days 3 and 10 with injections of either saline, noncovalent BiTEs (complexes)

or covalent BiTEs (conjugates) and sacrificed on day 16 for assessment of the extent of

metastatic disease. Compared to saline treated mice, which showed extensive tumor

growth with heavy melanin deposition over nearly 100% of the lung surface, animals

treated with complexes showed a modest reduction in tumor burden. However, animals

treated with covalently stabilized conjugates showed a substantially greater effect, with

only ~5% residual tumor compared to the saline treated controls (Fig. 3a).

We next assessed the effects of covalent BiTEs on tumor progression in a

localized subcutaneous implant model using MC38 colorectal carcinoma cells

expressing huHER2. Three days after tumor initiation by subcutaneous injection of cells

in the thigh, the animals received eight weekly i.v. injections of either noncovalent

complexes, covalently stabilized conjugates or saline. Most saline treated animals

showed rapid tumor growth, leading to death or mandatory sacrifice (i.e., following two

consecutive measurements of tumor volume >1 cm3, as required by protocol) within 30

days. Animals treated with complexes showed delayed tumor growth but continued

disease progression in most animals, consistent with previously published studies using

this model and a similar treatment regimen (16). In contrast, covalent conjugate treated

animals showed complete suppression of tumor growth in all cases (Fig. 3b) and

continued to gain weight normally during treatment (Fig. 3c). A modest prolongation of

survival was apparent in the complex treated animals, but substantially less than the

complete survival through day 80 in the conjugate treated group (Fig. 3d). Re-challenge

in these mice on day 80 with subcutaneous injection of 3×10^5 MC38-huHER2 cells

showed complete resistance to re-establishment of tumors, consistent with durable anti-

tumor recall immune responses.

Mechanisms of superior anti-tumor activity of covalent BiTEs

In vitro analysis showed that covalently stabilized conjugates were more potent than

complexes at inducing iNKT cell mediated lysis of huHER2 expressing tumor cells in

chromium release assays (Fig. 4a), possibly reflecting their greater stability. Similar

results were obtained using tumor spheroids cultured with either mouse or human iNKT

cells, with covalent conjugates generating greater levels of tumor cell killing and to

greater depth within the tumor cell mass (Fig. 4b). To assess the importance of the

specific targeting of the conjugated BiTE to huHER2, we grafted individual mice with

huHER2 positive and negative MC38 cells on opposite thighs. This showed partial

suppression of huHER2 negative tumors, while huHER2 positive tumors were

completely suppressed (Fig. 4c). Similarly, tumors established with mixtures of huHER2

positive and negative cells showed reduced efficacy of immunotherapy, which became

more pronounced as the fraction of huHER2 negative cells was increased

(Supplementary Fig. S4c). This indicated that at least part of the anti-tumor activity of

18

conjugated iNKT cell specific BiTEs was mediated by direct targeting to the tumor-associated antigen.

To further evaluate this point, we used two different approaches to assess the efficacy of conjugated BiTEs to target the glycolipid ligand to the huHER2 positive tumor. Using radiolabeled ^{14}C-C11:BP, we quantitated the delivery of conjugated BiTEs versus the free glycolipid to normal tissues and to established MC38-huHER2 tumors (Fig. 4d). This revealed higher and sustained accumulation of the glycolipid in tumor tissue compared to spleen and kidney when administered as conjugates. Liver tissue also showed relatively high levels of conjugates and free glycolipid initially, but this declined rapidly over time. A second approach using an azido modified variant of C11:BP enabled direct visualization of conjugates in tissue sections by fluorescent labelling (Supplementary Fig. S4d) (20). This confirmed the relatively high accumulation in liver and tumor tissues relative to spleen and kidney, without histologic evidence of tissue necrosis or inflammation in either tissue. Overall, these results suggested that specific targeting of conjugated BiTEs to tumors was relevant to improving anti-tumor effects by directing iNKT cell activation to the tumor site.

Analysis of TILs in conjugated BiTE treated mice

To gain further insight into the mechanisms for the superior anti-tumor effects of conjugated iNKT cell specific BiTEs, we carried out a detailed analysis of tumor infiltrating leukocytes (TILs). Tumors of MC38-huHER2 cells were first established to moderate size (0.3 cm^3) in the thigh, and the animals then received two injections of saline, complexes or conjugates (Fig. 5a). Representative tumors excised from these

animals were analyzed by routine histology and immunohistochemistry (Fig. 5b). This

revealed dense and well delineated tumors in all three treatment groups, with reduced

Ki67 staining and increased TUNEL positivity in the conjugated BiTE treated group,

indicative of reduced tumor cell proliferation and increased cell death. A notable finding

was the distribution of anti-CD3 staining, which was prominently confined to the margin

of the tumor in saline treated tumors, but evenly distributed throughout the tumor in

complex and conjugate treated tumors suggesting an effect on promoting T cell

infiltration. Extraction of TILs and FACS analysis (see Supplementary Fig. S5a and b for

gating strategy) revealed increased numbers of total leukocytes and T cells per gram of

tumor tissue in conjugated BiTE treated animals (Fig. 5c), and phenotypic analysis

showed an increase in the proportion of T cells lacking both CD4 and CD8 (i.e., double

negative (DN) T cells) (Fig. 5d). FoxP3$^+$ regulatory CD4$^+$ T cells (Treg) were reduced in

TILs from these animals (Fig. 5e). Significant effects on the composition of TILs with

regard to cell populations other than T cells were also observed in animals treated with

noncovalent complexes or conjugates. These included an increase in the proportion and

number of NK1.1$^+$ CD3 negative cells, most likely representing NK cells (Fig. 5f), and

significant effects on myeloid lineage cells with reductions in F4/80$^+$ macrophages and

Gr-1$^+$ neutrophils in conjugate treated tumors (Fig. 5g).

To functionally assess tumor specific T cell responses in TILs, we used an IFNγ

ELISPOT assay with stimulation by tumor lysate or synthetic peptides from the huHER2

tumor-associated antigen (Fig. 5h). Three peptides based on sequences of predicted

CD8$^+$ T cell epitopes in huHER2 were tested, with two of these generating significant

responses from T cells purified from tumors of conjugate treated mice, whereas no

significant responses were observed with T cells from tumors of animals treated with saline or noncovalent complexes. T cells from conjugate treated tumors responded to lysates of MC38-huHER2 cells, and also to lysate from MC38 cells not expressing huHER2, suggesting the stimulation of epitope spreading to endogenous mouse tumor associated antigens. All of the T cell responses detected in these assays were eliminated by depletion with anti-CD8 conjugated magnetic beads, implicating CD8^{+} T cells as the relevant effectors.

Analysis of iNKT cells in TILs

Based on αGalCer loaded CD1d tetramer staining, iNKT cells were present at similar numbers in TILs of tumors from saline, complex or conjugate treated mice (Fig. 6a). To assess the quality of these cells in the different treatment groups, we applied an extended multicolor analysis of 13 cell surface markers (see Fig. 6d for list) and three intracellular transcription factors (FoxP3, Tbet and RORγt). Dimensional reduction of the data to identify distinct populations of tetramer^{+} iNKT cells was carried out using t-distributed stochastic neighbor embedding (t-SNE) (Fig 6b) (35). The concatenated data from all three treatment groups revealed up to 20 distinct phenotypic clusters based on t-SNE-1 and t-SNE-2 two dimensional plots (Fig. 6c). These clusters could be separated into four distinct groups, based on their abundance in tumors from saline, complex or conjugate treated mice (Fig. 6d). Clusters comprising Group 1 were present exclusively in saline treated mice, while Group 2 subsets predominated in complex treated and Group 3 in conjugate treated animals. Subsets in Group 4 showed approximately equal levels in both complex and conjugate treated animals. Overall, this

analysis revealed a striking diversity of iNKT cells, suggesting a fine-tuning of their

functions when activated by different stimuli.

We also evaluated the previously established iNKT cell subsets based on

expression of CD4 and CD8 co-receptors, or their classification into NKT1, NKT2 and

NKT17 functional subsets based on intracellular transcription factor staining (36). We

observed a significant bias toward CD4 plus CD8 double positive (DP) iNKT cells in

TILs from complex treated mice, whereas this subset was nearly absent in conjugate

treated animals which had a greater predominance of CD4$^+$ and double negative (DN)

iNKT cells (Fig. 6e). With regard to functional subsets, all treatment groups had NKT2

cells as the majority population, and TILs from conjugated BiTE treated animals showed

significantly reduced proportions and numbers of NKT17 and increased proportions of

NKT1 cells (Fig. 6f and g).

Co-inhibitory receptors and checkpoint blockade in conjugated BiTE treatment

We also analyzed expression of costimulatory and co-inhibitory receptors on iNKT cells

from our multiparameter analysis of TILs (Fig. 7a). Compared to saline treated mice,

conjugated BiTEs gave no significant increase in expression of costimulatory receptors

4-1BB, ICOS, OX40 or CD28 on iNKT cells, although the expression was distributed in

different clusters based on t-SNE analysis. With regard to co-inhibitory receptors, both

complexes and conjugates induced higher expression of CTLA-4, but no change or a

reduction in LAG3 (CD223), PD-1 (CD279) or Tim-3. This increase in CTLA-4

expression was consistent with the increase in this receptor observed in liver iNKT cells

following treatment with conjugated BiTEs (Fig. 2c). Given these findings, we performed

experiments to assess synergy between anti-CTLA4 and conjugated BiTEs in the

MC38-huHER2 model using both wild type C57BL/6 mice (Supplementary Fig. S6) or

human CD1d knock-in mice (Fig. 7). The latter represent a potentially more accurate

model for translational studies, since they closely resemble humans with regard to

numbers of iNKT cells and the strength of responses to iNKT cell activators (21, 37).

Animals implanted with subcutaneous MC38-huHER2 tumors received three weekly i.v.

injections of conjugated BiTEs and i.p. injections of either 100 μg of hamster anti-CTLA-

4 or control normal hamster serum IgG (Fig. 7b). Under these conditions, conjugates

alone were ineffective and anti-CTLA-4 alone had a small impact on tumor progression.

However, strong synergy was observed with the combination of conjugates plus

concurrent anti-CTLA-4 (Figs. 7c,d). A similar pattern of responses with synergy

between conjugates and anti-CTLA-4 checkpoint blockade was also observed in wild

type C57BL/6 mice (Supplementary Fig. S6a-d).

Discussion

The discovery of αGalCer as a powerful anti-tumor agent in mice (38), and its

subsequent identification as a specific activator of iNKT cells (39), triggered substantial

interest in the potential for iNKT cell directed cancer immunotherapy (9, 40, 41). While

treatment with free αGalCer shows remarkable anti-tumor activity in mouse models,

phase I clinical trials of this approach in human cancer patients have not shown clear

evidence of therapeutic benefit (11, 34, 42, 43). Several problems confronting iNKT cell

therapies have been identified, including depletion and dysfunction of these cells in

cancer patients (44), and the tendency of strong activators such as αGalCer to induce a

long-lasting anergic state (14, 32, 45, 46). The induction of anergy is a major limitation for regimens that depend on repetitive stimulation of iNKT cells to achieve strong and durable effects against established cancers. In addition, systemic administration of free glycolipid activators of iNKT cells has been linked to major toxic effects in mouse models, including severe hepatic necrosis and potentiation of septic shock (15, 47, 48). These observations indicate the need for new approaches for delivering iNKT cell activators more selectively to the tumor microenvironment while avoiding the induction of anergy.

An approach for creating more targetable iNKT cell activators is the use of soluble CD1d proteins loaded *ex vivo* with αGalCer (16, 17). However, this approach is compromised by the inherent instability of the glycolipid-protein complex, which is prone to rapid dissociation *in vivo*. To overcome this issue, we created covalent conjugates of αGalCer with soluble CD1d proteins as stable and specific bispecific iNKT cell engagers (20). The current study assessed the *in vivo* immune activation resulting from systemic injection of these covalently stabilized BiTEs, and their potential for anti-tumor immunotherapy. We found that conjugated BiTEs had a unique ability to optimally activate multiple immunological functions of iNKT cells while inducing only minor levels of iNKT cell expansion, and little or no hypo-responsiveness to subsequent stimulation. Compared to responses stimulated by systemic injection of free αGalCer, the iNKT cell responses to a single injection of BiTEs showed rapid and strong induction of multiple iNKT cell effector functions and upregulation of activation related molecules.

Responses to iNKT cell specific BiTEs did not require presentation by CD1d on APCs, which contrasts strongly with free αGalCer which requires presentation by

CD1d+ cells, most prominently CD8α[+] DEC205^{+} DCs in mice (4). It was also notable

that activation of iNKT cell cytokine secretion appeared to occur without any specific

anchoring of the BiTEs to an APC surface, as shown in mice lacking any expression of

human HER2. The ability of a soluble TCR ligand to strongly stimulate cytokine

production without multimerization or anchoring to an APC surface was surprising, and

suggests that iNKT cells may be less dependent on costimulatory signals than

conventional T cells for stimulation of effector functions. This may also be relevant to

the lack of anergy following stimulation with conjugated BiTEs, as anergy of iNKT cells

is potentiated when TCR stimulation is accompanied by costimulation through CD28

and ICOS, the two principle costimulatory receptors known to be active on iNKT cells

(45, 46, 48). Thus, our ability to activate iNKT cells without direct presentation by APCs

should bypass these costimulatory signals, explaining the lack of proliferative expansion

or anergy. In addition, the ligands for multiple costimulatory and co-inhibitory receptors

were less strongly upregulated on APCs by iNKT cell specific BiTEs compared to free

αGalCer, which may have further reduced the induction or maintenance of anergy

following iNKT cell activation.

In spite of the relatively similar effects of nonconjugated and conjugated BiTEs in

activating iNKT cell responses, there were markedly superior anti-tumor responses with

covalent conjugates in our experiments, or when compared to published results using

similar noncovalent complexes (16, 17). This can be explained by the partial induction

of hypo-responsiveness by multiple injections of complexes (16), which was attributed

to the ability of glycolipid to dissociate from the CD1d protein and stimulate APC-

dependent responses (19). The more stable covalently conjugated BiTEs minimized or

eliminated this problem, leading to improvements in the anti-tumor immune response including recruitment of direct cytotoxicity toward tumor cells, enhanced cross-priming of $CD8^+$ T cells and improved T cell penetration into tumors. With regard to iNKT cells within the TILs, t-SNE analysis revealed substantial heterogeneity with several distinct phenotypic clusters that distinguished noncovalent complex and conjugated BiTE treated mice. Although the functions of the different populations identified by this analysis remain to be investigated, a number of provocative findings were evident. For example, the presence of a distinctive $CD8\alpha^+$ subset (cluster 2) exclusively in complex treated animals could indicate a subset that is deleterious to the highly effective antitumor response induced by conjugated BiTEs. Conversely, the presence of several distinct subsets comprising Group 3 clusters may point to specific subsets or differentiation states of iNKT cells that drive anti-tumor immunity.

Our studies on combinations of iNKT cell specific conjugated BiTE injections and anti-CTLA-4 antibodies provided initial proof of concept for adding checkpoint blockade to an optimized iNKT cell activating regimen. Our choice of CTLA-4 blockade was guided in part by the increased expression of this receptor observed on iNKT cell populations in tumors of conjugated BiTE treated animals. However, given our observations of the upregulation of multiple inhibitory receptors within TILs and in other tissues of tumor bearing mice, it will be prudent to test additional combinations using other checkpoint blockade agents such as anti-PD-1/PD-L1 and anti-LAG3. Checkpoint blockade may improve responses by other cell types that are stimulated downstream of iNKT cell activation, in particular $CD8^+$ anti-tumor cytolytic T cells. Our finding that peptide specific $CD8^+$ T cell responses against tumor associated antigens were

increased by conjugated BiTE treatment provides further incentives to explore

combinations with checkpoint blockade strategies, and also for adding therapeutic

tumor vaccines. While our results confirm the known direct tumoricidal activities of iNKT

cells, the secondary effects of the conjugated BiTEs on enhancing tumor-specific CD8$^+$

T cell priming as well as NK cell activation strongly suggests that these cells also

contribute as terminal effectors in the potent anti-tumor effects observed in our model

system. Determining the relative importance of these and other potential effector

populations in animals treated with iNKT cell specific BiTEs will be a focus for future

analysis, along with more detailed assessment of efficacy of our approach in models

that more accurately represent clinically relevant scenarios for cancer treatment.

The production of covalently stabilized conjugated BiTEs and the validation of

their immunostimulatory properties provide a promising new avenue for iNKT cell

directed therapy, although several major challenges remain. One of these is the

apparent need for tumor-specific targeting of the conjugates to achieve maximal

therapeutic effects, which imposes limitations on the types of cancers that can be

effectively treated. However, the huHER2 protein that served as the target for our

preclinical studies is expressed by a substantial fraction of breast cancers, and is one of

several well-established targets for clinical translation of our approach. Targets could

also include normal cell surface antigens with a restricted range of expression such as

CD19, which has recently been demonstrated as an effective target for αGalCer-loaded

CD1d complexes in mouse models of tumor immunotherapy (49). In addition, while

conjugated BiTEs were most effective in our studies when designed to specifically bind

to the tumor cell surface, partial effects were observed against tumors lacking the

specifically targeted tumor antigen (Fig. 4c). Further work is ongoing to assess the potential for non-targeted conjugates, especially in combination immunotherapy regimens for tumors lacking known surface targets.

Our studies have not directly compared the anti-tumor potential of iNKT cell engaging BiTEs to many other bispecific T cell engagers that may more broadly stimulate effector T cells, such as BiTEs that act through binding to CD3 to more promiscuously activate all T cells. These latter constructs represent a potent family of T cell activators, although their potential toxicities remain a major concern that may limit their efficacy (50). In contrast, the relatively low numbers of iNKT cells in normal humans, and their further reduction and loss of function in many cancer patients (11, 51), suggest that iNKT cell selective BiTEs are likely to be better tolerated, albeit less potent than more broadly acting T cell engagers. In this regard, it is encouraging that strong anti-tumor effects with iNKT cell engaging BiTEs were seen in our experiments with human CD1d knock-in mice, despite their low numbers of iNKT cells (37). These effects could potentially be amplified by combining iNKT cell selective conjugated BiTEs with strategies for increasing iNKT cell numbers and function, such as adoptive cell therapy for engineering of chimeric antigen receptor expressing iNKT cells (9, 52). These and other approaches are becoming increasingly feasible, and are likely to converge in the future to generate practical and effective methods for iNKT cell based immunotherapy of cancer.

Acknowledgements

References

1. Brennan PJ, Brigl M, Brenner MB. Invariant natural killer T cells: an innate activation scheme linked to diverse effector functions. Nat Rev Immunol. 2013;13: 101-17.

2. Rossjohn J, Pellicci DG, Patel O, Gapin L, Godfrey DI. Recognition of CD1d-restricted antigens by natural killer T cells. Nat Rev Immunol. 2012;12: 845-57.

3. Carreno LJ, Saavedra-Avila NA, Porcelli SA. Synthetic glycolipid activators of natural killer T cells as immunotherapeutic agents. Clin Transl Immunology. 2016;5: e69.

4. Arora P, Baena A, Yu KO, Saini NK, Kharkwal SS, Goldberg MF, et al. A single subset of dendritic cells controls the cytokine bias of natural killer T cell responses to diverse glycolipid antigens. Immunity. 2014;40: 105-16.

5. Godfrey DI, Le Nours J, Andrews DM, Uldrich AP, Rossjohn J. Unconventional T Cell Targets for Cancer Immunotherapy. Immunity. 2018;48: 453-73.

6. Hong C, Lee H, Park YK, Shin J, Jung S, Kim H, et al. Regulation of secondary antigen-specific CD8(+) T-cell responses by natural killer T cells. Cancer Res. 2009;69: 4301-8.

7. Laurent X, Bertin B, Renault N, Farce A, Speca S, Milhomme O, et al. Switching invariant natural killer T (iNKT) cell response from anticancerous to anti-inflammatory effect: molecular bases. J Med Chem. 2014;57: 5489-508.

8. Bedard M, Salio M, Cerundolo V. Harnessing the Power of Invariant Natural Killer T Cells in Cancer Immunotherapy. Front Immunol. 2017;8: 1829.

9. Wolf BJ, Choi JE, Exley MA. Novel Approaches to Exploiting Invariant NKT Cells in Cancer Immunotherapy. Front Immunol. 2018;9: 384.

10. Exley MA, Nakayama T. NKT-cell-based immunotherapies in clinical trials. Clin Immunol. 2011;140: 117-8.

11. Nair S, Dhodapkar MV. Natural Killer T Cells in Cancer Immunotherapy. Front Immunol. 2017;8: 1178.

12. Waldowska M, Bojarska-Junak A, Rolinski J. A brief review of clinical trials involving manipulation of invariant NKT cells as a promising approach in future cancer therapies. Cent Eur J Immunol. 2017;42: 181-95.

13. Im JS, Arora P, Bricard G, Molano A, Venkataswamy MM, Baine I, et al. Kinetics and cellular site of glycolipid loading control the outcome of natural killer T cell activation. Immunity. 2009;30: 888-98.

14. Parekh VV, Wilson MT, Olivares-Villagomez D, Singh AK, Wu L, Wang CR, et al. Glycolipid antigen induces long-term natural killer T cell anergy in mice. J Clin Invest. 2005;115: 2572-83.

15. Singh M, Quispe-Tintaya W, Chandra D, Jahangir A, Venkataswamy MM, Ng TW, et al. Direct incorporation of the NKT-cell activator alpha-galactosylceramide into a recombinant Listeria monocytogenes improves breast cancer vaccine efficacy. Br J Cancer. 2014;111: 1945-54.

16. Corgnac S, Perret R, Derre L, Zhang L, Stirnemann K, Zauderer M, et al. CD1d-antibody fusion proteins target iNKT cells to the tumor and trigger long-term therapeutic responses. Cancer Immunol Immunother. 2013;62: 747-60.

17. Stirnemann K, Romero JF, Baldi L, Robert B, Cesson V, Besra GS, et al. Sustained activation and tumor targeting of NKT cells using a CD1d-anti-HER2-scFv fusion protein induce antitumor effects in mice. J Clin Invest. 2008;118: 994-1005.

18. Slaney CY, Wang P, Darcy PK, Kershaw MH. CARs versus BiTEs: A Comparison between T Cell-Redirection Strategies for Cancer Treatment. Cancer Discov. 2018;8: 924-34.

19. Zhang L, Donda A. Alpha-Galactosylceramide/CD1d-Antibody Fusion Proteins Redirect Invariant Natural Killer T Cell Immunity to Solid Tumors and Promote Prolonged Therapeutic Responses. Front Immunol. 2017;8: 1417.

20. Veerapen N, Kharkwal SS, Jervis P, Bhowruth V, Besra AK, North SJ, et al. Photoactivable Glycolipid Antigens Generate Stable Conjugates with CD1d for Invariant Natural Killer T Cell Activation. Bioconjug Chem. 2018;29: 3161-73.

21. Wen X, Rao P, Carreno LJ, Kim S, Lawrenczyk A, Porcelli SA, et al. Human CD1d knock-in mouse model demonstrates potent antitumor potential of human CD1d-restricted invariant natural killer T cells. Proc Natl Acad Sci U S A. 2013;110: 2963-8.

22. Khurana A, Kronenberg M. A method for production of recombinant mCD1d protein in insect cells. J Vis Exp. 2007: 556.

23. Im JS, Yu KO, Illarionov PA, LeClair KP, Storey JR, Kennedy MW, et al. Direct measurement of antigen binding properties of CD1 proteins using fluorescent lipid probes. J Biol Chem. 2004;279: 299-310.

24. Yu KO, Im JS, Illarionov PA, Ndonye RM, Howell AR, Besra GS, et al. Production and characterization of monoclonal antibodies against complexes of the NKT cell ligand alpha-galactosylceramide bound to mouse CD1d. J Immunol Methods. 2007;323: 11-23.

25. Dong ZJ, Wei HM, Sun R, Tian ZG, Gao B. Isolation of murine hepatic lymphocytes using mechanical dissection for phenotypic and functional analysis of NK1.1+ cells. World J Gastroenterol. 2004;10: 1928-33.

26. Arora P, Venkataswamy MM, Baena A, Bricard G, Li Q, Veerapen N, et al. A rapid fluorescence-based assay for classification of iNKT cell activating glycolipids. J Am Chem Soc. 2011;133: 5198-201.

27. Bricard G, Venkataswamy MM, Yu KO, Im JS, Ndonye RM, Howell AR, et al. Alpha-galactosylceramide analogs with weak agonist activity for human iNKT cells define new candidate anti-inflammatory agents. PLoS One. 2010;5: e14374.

28. Schneider CA, Rasband WS, Eliceiri KW. NIH Image to ImageJ: 25 years of image analysis. Nat Methods. 2012;9: 671-5.

29. Faustino-Rocha A, Oliveira PA, Pinho-Oliveira J, Teixeira-Guedes C, Soares-Maia R, da Costa RG, et al. Estimation of rat mammary tumor volume using caliper and ultrasonography measurements. Lab Anim (NY). 2013;42: 217-24.

30. Jensen MM, Jorgensen JT, Binderup T, Kjaer A. Tumor volume in subcutaneous mouse xenografts measured by microCT is more accurate and reproducible than determined by 18F-FDG-microPET or external caliper. BMC Med Imaging. 2008;8: 16.

31. Jeon J, Kang JA, Shim HE, Nam YR, Yoon S, Kim HR, et al. Efficient method for iodine radioisotope labeling of cyclooctyne-containing molecules using strain-promoted copper-free click reaction. Bioorg Med Chem. 2015;23: 3303-8.

32. Wilson MT, Johansson C, Olivares-Villagomez D, Singh AK, Stanic AK, Wang CR, et al. The response of natural killer T cells to glycolipid antigens is characterized by surface receptor down-modulation and expansion. Proc Natl Acad Sci U S A. 2003;100: 10913-8.

33. Wingender G, Birkholz AM, Sag D, Farber E, Chitale S, Howell AR, et al. Selective Conditions Are Required for the Induction of Invariant NKT Cell Hyporesponsiveness by Antigenic Stimulation. J Immunol. 2015;195: 3838-48.

34. Giaccone G, Punt CJ, Ando Y, Ruijter R, Nishi N, Peters M, et al. A phase I study of the natural killer T-cell ligand alpha-galactosylceramide (KRN7000) in patients with solid tumors. Clin Cancer Res. 2002;8: 3702-9.

35. Toghi Eshghi S, Au-Yeung A, Takahashi C, Bolen CR, Nyachienga MN, Lear SP, et al. Quantitative Comparison of Conventional and t-SNE-guided Gating Analyses. Front Immunol. 2019;10: 1194.

36. Lee YJ, Wang H, Starrett GJ, Phuong V, Jameson SC, Hogquist KA. Tissue-Specific Distribution of iNKT Cells Impacts Their Cytokine Response. Immunity. 2015;43: 566-78.

37. Chennamadhavuni D, Saavedra-Avila NA, Carreno LJ, Guberman-Pfeffer MJ, Arora P, Yongqing T, et al. Dual Modifications of alpha-Galactosylceramide Synergize to Promote Activation of Human Invariant Natural Killer T Cells and Stimulate Anti-tumor Immunity. Cell Chem Biol. 2018;25: 571-84 e8.

38. Motoki K, Morita M, Kobayashi E, Uchida T, Akimoto K, Fukushima H, et al. Immunostimulatory and antitumor activities of monoglycosylceramides having various sugar moieties. Biol Pharm Bull. 1995;18: 1487-91.

39. Kawano T, Cui J, Koezuka Y, Toura I, Kaneko Y, Motoki K, et al. CD1d-restricted and TCR-mediated activation of valpha14 NKT cells by glycosylceramides. Science. 1997;278: 1626-9.

40. Krijgsman D, Hokland M, Kuppen PJK. The Role of Natural Killer T Cells in Cancer-A Phenotypical and Functional Approach. Front Immunol. 2018;9: 367.

41. Godfrey DI, Kronenberg M. Going both ways: immune regulation via CD1d-dependent NKT cells. J Clin Invest. 2004;114: 1379-88.

42. Kunii N, Horiguchi S, Motohashi S, Yamamoto H, Ueno N, Yamamoto S, et al. Combination therapy of in vitro-expanded natural killer T cells and alpha-galactosylceramide-pulsed antigen-presenting cells in patients with recurrent head and neck carcinoma. Cancer Sci. 2009;100: 1092-8.

43. Ishikawa A, Motohashi S, Ishikawa E, Fuchida H, Higashino K, Otsuji M, et al. A phase I study of alpha-galactosylceramide (KRN7000)-pulsed dendritic cells in patients with advanced and recurrent non-small cell lung cancer. Clin Cancer Res. 2005;11: 1910-7.

44. Singh AK, Shukla NK, Das SN. Altered invariant natural killer T cell subsets and its functions in patients with oral squamous cell carcinoma. Scand J Immunol. 2013;78: 468-77.

45. Singh AK, Gaur P, Das SN. Natural killer T cell anergy, co-stimulatory molecules and immunotherapeutic interventions. Hum Immunol. 2014;75: 250-60.

46. Iyoda T, Ushida M, Kimura Y, Minamino K, Hayuka A, Yokohata S, et al. Invariant NKT cell anergy is induced by a strong TCR-mediated signal plus co-stimulation. Int Immunol. 2010;22: 905-13.

47. Ando T, Ito H, Ohtaki H, Kanbe A, Hirata A, Hara A, et al. Role of invariant NKT cells in lipopolysaccharide-induced lethal shock during encephalomyocarditis virus infection. Immunobiology. 2017;222: 350-7.

48. Ito H, Koide N, Hassan F, Islam S, Tumurkhuu G, Mori I, et al. Lethal endotoxic shock using alpha-galactosylceramide sensitization as a new experimental model of septic shock. Lab Invest. 2006;86: 254-61.

49. Das R, Guan P, Wiener SJ, Patel NP, Gohl TG, Evans E, et al. Enhancing the antitumor functions of invariant natural killer T cells using a soluble CD1d-CD19 fusion protein. Blood Adv. 2019;3: 813-24.

50. Ellerman D. Bispecific T-cell engagers: Towards understanding variables influencing the in vitro potency and tumor selectivity and their modulation to enhance their efficacy and safety. Methods. 2019;154: 102-17.

51. Molling JW, Kolgen W, van der Vliet HJ, Boomsma MF, Kruizenga H, Smorenburg CH, et al. Peripheral blood IFN-gamma-secreting Valpha24+Vbeta11+ NKT cell numbers are decreased in cancer patients independent of tumor type or tumor load. Int J Cancer. 2005;116: 87-93.

52. Bollino D, Webb TJ. Chimeric antigen receptor-engineered natural killer and natural killer T cells for cancer immunotherapy. Transl Res. 2017;187: 32-43.

Figure Legends

Figure 1; *In vivo* **activities of iNKT cell specific BiTEs. (a)** Intracellular IFNγ staining of iNKT cells 8 or 16 hr post i.v. injection of WT (C57BL/6) mice with 1 nanomole of conjugates, complexes, free glycolipids (C11:BP or C26:0) or saline. **(b)** Serum IFNγ in CD1d-/- mice 12 hr post i.v. injection with vehicle, free glycolipid or conjugates with or without adoptive transfer of 100,000 purified iNKT cells from WT mice 16 hours earlier. **(c)** Surface modulation of activation related markers on splenic iNKT cells in WT mice

injected once i.v. with 1 nanomole of free glycolipid (C26:0), complexes or conjugates, and sacrificed at indicated times for staining with αGalCer-loaded mCD1d tetramers and antibodies to surface molecules. Values are plotted as fold change in MFI compared to untreated controls. **(d)** Serum cytokine levels in WT mice following injection of free glycolipid, complexes or conjugates. **(e)**. Expansion kinetics of iNKT cells in WT mice following a single i.v. injection of free glycolipid (C26:0), complexes or conjugates were determined by FACS analysis of splenocytes. Results are plotted as percent of total splenic TCRβ and Tetramer$^+$ cells. Dashed line shows baseline level in saline injected animals. **P < 0.01, *** P < 0.001, ****P < 0.0001; 2-way ANOVA with Sidak multiple comparison test. All symbols or bars show means ± 1 SE for groups of 3 mice, and data are representative of at least three separate experiments.

Figure 2; Reduced anergy and exhaustion of iNKT cells following stimulation by conjugates. (a) Mice were primed with i.v. injections of vehicle, free glycolipid (C26:0), complexes or conjugates either once or three times at weekly intervals. One week later, all groups were re-stimulated with i.v. C26:0, and serum IFNγ was measured at 12 hours by ELISA. **(b)** Quantitation of iNKT cells as percentage of total T cells by tetramer staining of splenocytes harvested at 72 hours after priming and restimulation as in panel A. **(c)** Surface expression of inhibitory checkpoint receptors by iNKT cells was measured on spleen and liver on tetramer stained iNKT cells 48 hours after the second of two weekly injections of saline versus conjugates. **(d)** Upregulation of ligands for co-inhibitory receptors on spleen CD11c+ DCs after stimulation with free glycolipid, complexes or conjugates. Data are means ± 1 SE for groups of 3 – 5 mice, and are

representative of at least three experiments. *P < 0.05; **P < 0.01; ***P < 0.001; ****p<0.0001, 2-way ANOVA with Sidak multiple comparisons test.

Figure 3; Enhancement of tumor immunotherapy with conjugates. (a) Schematic for tumor injection and immunotherapy for B16.F10-huHER2 tumor model. Images of lungs harvested on day 16 from 5 mice per treatment group are shown, and extent of tumor growth was calculated as percent lung surface covered with melanized nodules. Bars show means ± 1 SE. **P < 0.01, ****p<0.0001; 2-way ANOVA with Sidak multiple comparisons test. **(b)** Schematic for grafting MC38-huHER2 and immunotherapy regimen. Tumor growth curves for individual mice in each treatment group are shown for groups of 8 – 10 mice. Numbers of complete responders (CR) with no detectable tumor are indicated. **(c)** Comparison of weight change from day of tumor graft to day 30 in mice treated with huHER2 targeted complexes or conjugates. **P < 0.01; 2-way ANOVA. **(d)** Survival curves for treatment groups. **P < 0.01; log rank test.

Figure 4; Specific cytotoxicity and tissue deposition of HER2-targeted conjugates. (a) MC38-huHER2 cells labeled with ^{51}Cr labeled were incubated with anti-huHER2 conjugates or complexes. Target specific killing was determined following incubation for 12 hr with human iNKT cell clone HDD3 at effector:target ratio of 1:1. **(b)** Spheroids of MC38-huHER2 cells were pulsed with saline or anti-huHER2 complexes or conjugates containing either murine (top) or human (bottom) CD1d. Following incubation for 12 hr with mouse spleen iNKT cells (top) or human iNKT cells (clone HDD3, bottom), spheroids were stained for markers of viability, apoptosis and necrosis.

Scale bar 1 mm. **(c)** Mice were grafted on day 0 with 5 x 10^5 MC38-huHER2 cells s.c. in the right thigh and 5 x 10^5 huHER2 negative MC38 cells in the left thigh. Injections of saline or anti-huHER2 conjugates were given i.v. on days 3, 10 and 17, and growth of tumors on left and right thighs was followed to day 30. **(d)** Mice grafted with 5 x 10^5 MC38-huHER2 tumor cells 14 days earlier received a single i.v. injection of 1 nanomole of anti-HER2 conjugates loaded with ^{14}C-labelled C11:BP glycolipid or 1 nanomole of ^{14}C-labeled free C11:BP glycolipid. Individual mice were sacrificed at times shown, and ^{14}C retention in organ or tumor tissues was determined by liquid scintillation counting. Dashed lines indicate background CPM for mice injected with saline only. *P < 0.05, **P < 0.01 ***P < 0.001, ****P < 0.0001, 2-way ANOVA with Sidak multiple comparison test.

Figure 5; T cell infiltrates of tumors treated with iNKT cell specific BiTEs. (a) Protocol for generation of tumors for TIL extraction and analysis in mice injected with saline versus huHER2-specific complexes or conjugates. **(b)** Immunohistochemistry of representative tumors from treated mice. **(c)** Quantitation of total TILs (CD45$^+$) and T cells (CD3$^+$) by FACS in tumors from treated mice (N = 5 mice per group). **(d)** Diagrams showing relative proportions of T cell subsets based on CD4 and CD8 expression, including double negative (DN) and double positive (DP) subsets. The size of each circle is proportional to the total T cell number in TILs for each treatment group. **(e)** Percentage of FoxP3$^+$ CD25$^+$ Tregs among total CD3$^+$ cells in TILs. **(f)** Percentage of CD3 negative NK1.1$^+$ cells among CD45$^+$ TILs. **(g)** Myeloid subsets showing percentages of F4/80$^+$ (macrophages) and Gr1$^+$ (granulocytes) among total CD11b$^+$ cells in TILs. **(h)** ELISPOT assay showing IFNγ spot forming cells in purified total T cells

(left) and CD8 depleted T cells (right) from spleens of MC38-huHER2 tumor bearing mice injected twice with saline, complexes or conjugates and re-stimulated *ex vivo* with lysates of MC38, MC38-huHER2, synthetic peptides spanning three predicted MHC class I presented epitopes of huHER2, or PMA plus Ionomycin. Bars show means and range for values from two mice for each treatment group. N = 6 mice per treatment group for c – g, *P < 0.05, **P < 0.01, ***P < 0.001, 2-way ANOVA with Sidak multiple comparison test.
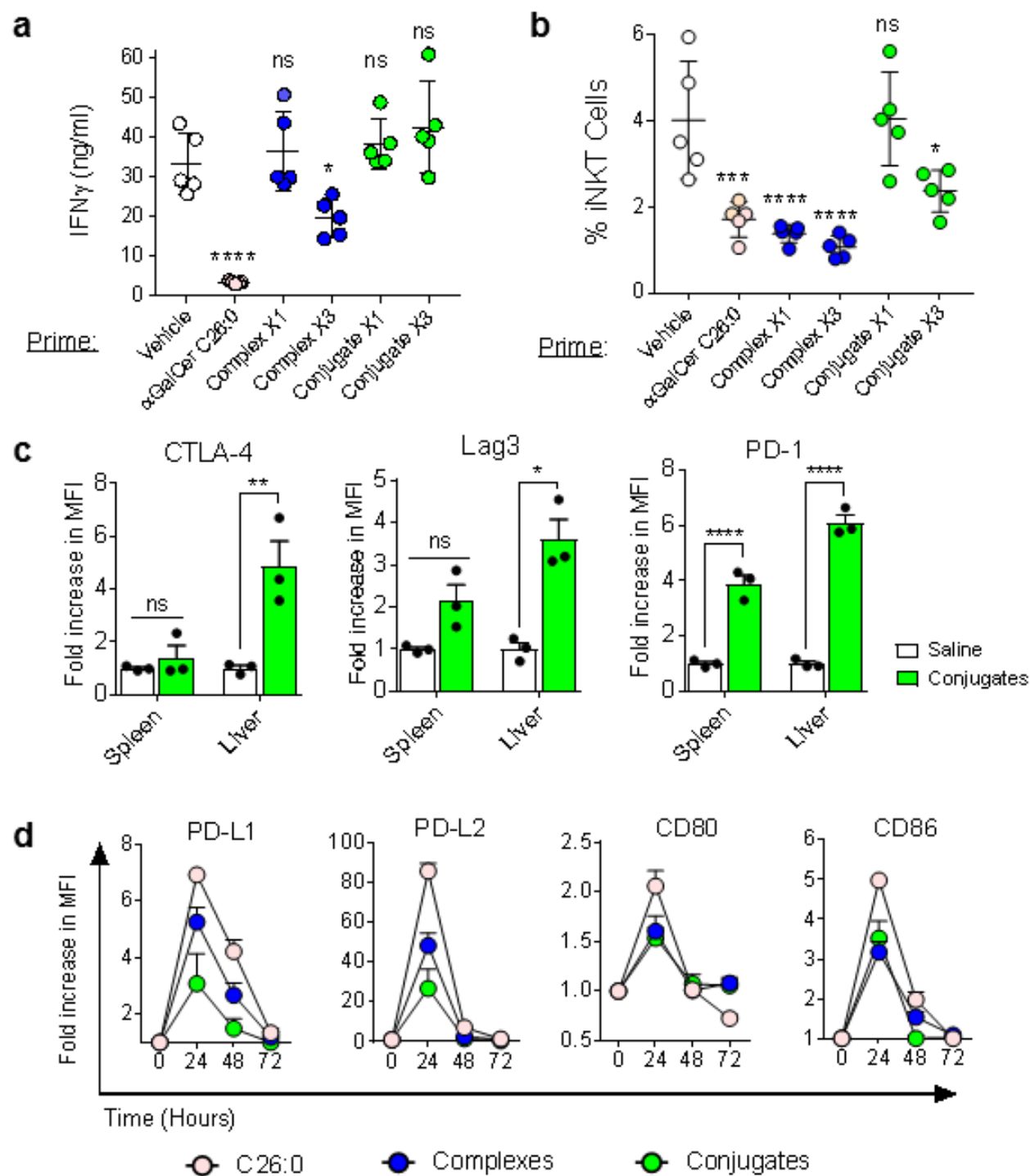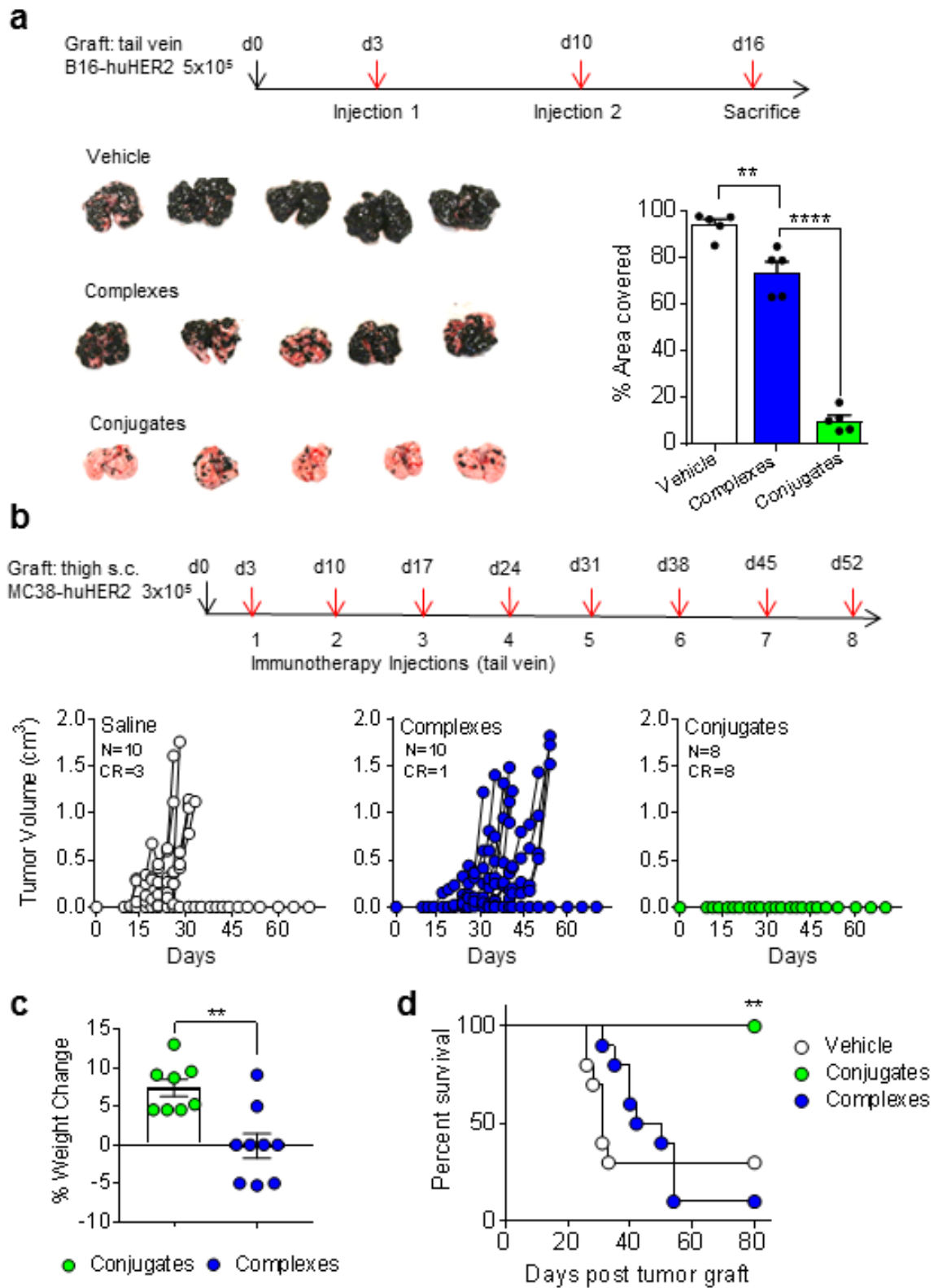
Figure 6; Analysis of iNKT cells in TILs. (a) Gating of iNKT cells in TILs and quantitation of absolute numbers of iNKT cells in total TILs extracted per tumor from mice with MC38-huHER2 tumors and treatments as in Fig. 5 (ns, not significant; 2-way ANOVA). **(b)** Two dimensional plots from t-SNE analysis of tetramer+ iNKT cells in TILs based on expression of 16 markers (listed in panel d). **(c)** Concatenated t-SNE analysis for all three treatment groups identifying 20 phenotypic clusters of iNKT cells. **(d)** Identification of four distinct groups of iNKT cells in TILs based on clustering by t-SNE. Bar graph on top shows relative abundance for each cluster in TILs of each treatment group. Heat map shows level of expression (normalized MFI) for each marker analyzed. **(e)** Subsets of CD4 and CD8α single positive, double positive (DP) and double negative (DN) expressing iNKT cells from t-SNE analysis mapped onto the concatenated data set (grey) in colors corresponding to each treatment group (red for saline, blue for complexes and green for conjugates). Pie charts show relative proportions of each subset by treatment group. **(f)** Similar to panel E, except showing distribution of signature transcription factors for functional iNKT cell subsets (i.e., classified as NKT1,
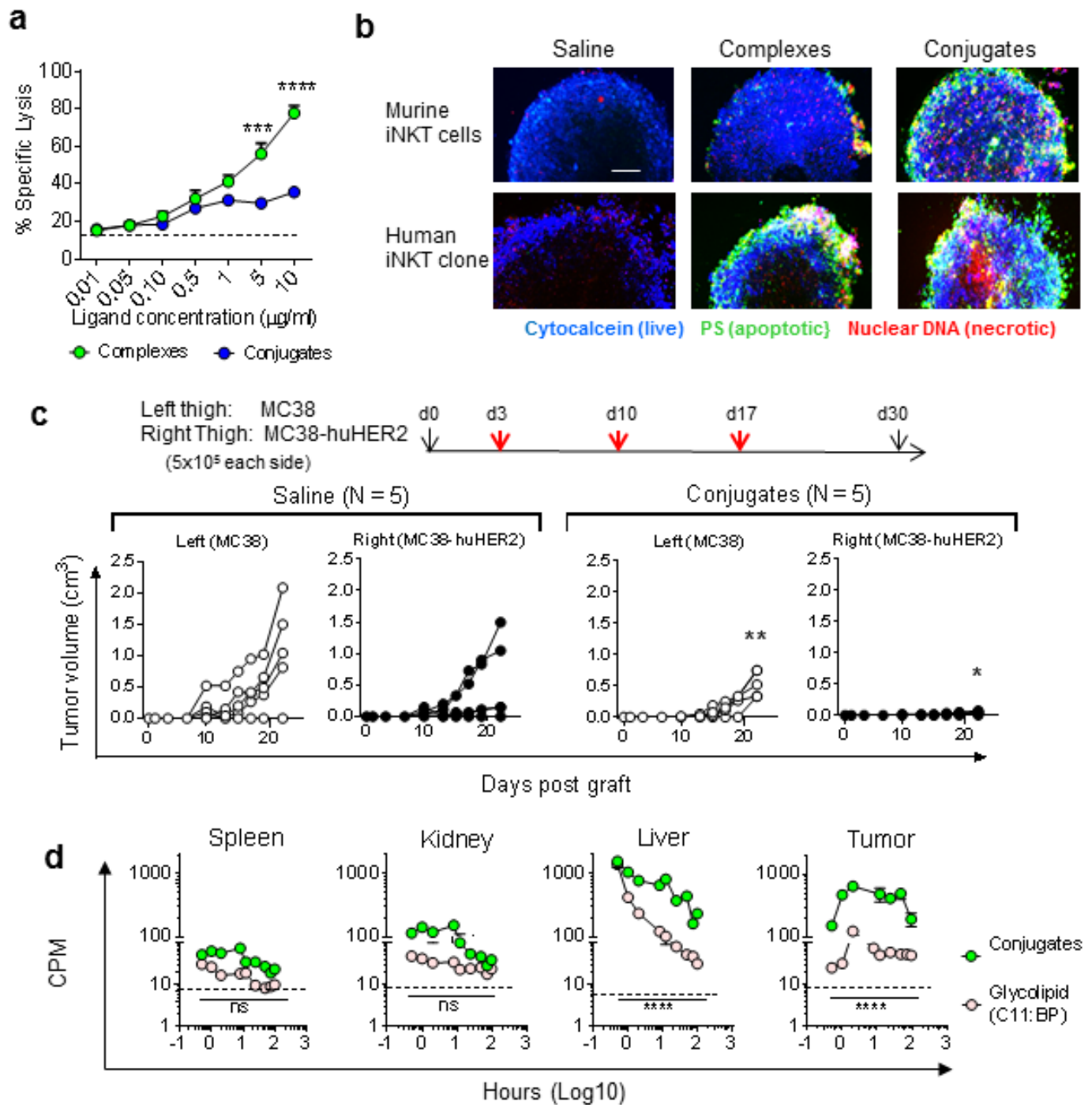
NKT2 or NKT17 based on Tbet and RORγt as previously described[36]). **(g)** Bar graph on left shows absolute numbers of iNKT cells in total TILs isolated per tumor. *P < 0.05 for NKT17 cells in conjugate group compared to saline controls. Other trends observed did not reach statistical significance. Stacked bar graph on right shows subsets as percentage of total iNKT cells. Means ± 1SE for treatment groups are shown. ***P < 0.01, ****P < 0.001; 2-way ANOVA with Sidak multiple comparison test. All analyses based on data from 6 mice per group

Figure 7; Synergistic antitumor effects of conjugates combined with checkpoint blockade. (a) Expression of costimulatory and co-inhibitory checkpoint receptors on iNKT cells in TILs from saline (red), complex (blue) or conjugate (green) treated mice. Graphs show fold increase compared to mean values for MFI in saline treated mice. **(b)** Scheme for combination treatment of MC38-huHER2 tumor bearing human CD1d knock-in mice with conjugates plus anti-CTLA-4 blocking antibody. For experiments using human CD1d knock-in mice, the conjugates also contained human CD1d. **(c)** Tumor growth shown as mean values for each treatment group (N = 6 – 8 mice per group). **(d)** Tumor growth curves for individual mice in each treatment group. The numbers of tumor free mice remaining at the end of observation at day 36 are indicated. *P < 0.05, **P < 0.01, ***P < 0.001, ****P < 0.0001; ns, not significant; 2-way ANOVA with Sidak multiple comparison test.

Figure 1

Figure 2

Figure 3

Figure 4

a

% Specific Lysis

Ligand concentration (µg/ml)

- Complexes
- Conjugates

b

	Saline	Complexes	Conjugates
Murine iNKT cells			
Human iNKT clone			

Cytocalcein (live)   PS (apoptotic)   Nuclear DNA (necrotic)

c

Left thigh: MC38
Right Thigh: MC38-huHER2
(5x10^5 each side)

d0   d3   d10   d17   d30

Saline (N = 5)   Conjugates (N = 5)

Left (MC38)   Right (MC38-huHER2)   Left (MC38)   Right (MC38-huHER2)

Tumor volume (cm^3)

** *

Days post graft

d

Spleen   Kidney   Liver   Tumor

CPM

ns   ns   ****   ****

Hours (Log10)

- Conjugates
- Glycolipid (C11:BP)

Figure 5

Figure 6

Figure 7

a

b

Graft: thigh s.c.
MC38-huHER2 3 x 10⁵

Conjugates or saline

d3   d10   d17

Day 0

N = 6-8 mice / group
(human CD1d knock-in)

d3   d10   d17

αCTLA-4 or control IgG

c

○ Saline
● antiCTLA4
● Conjugates + Ctrl IgG
● Conjugates + antiCTLA4

d

Saline — N=6, Tumor free=0

Conjugates + Ctrl IgG — N=7, Tumor free=1

anti-CTLA-4 — N=6, Tumor free=1

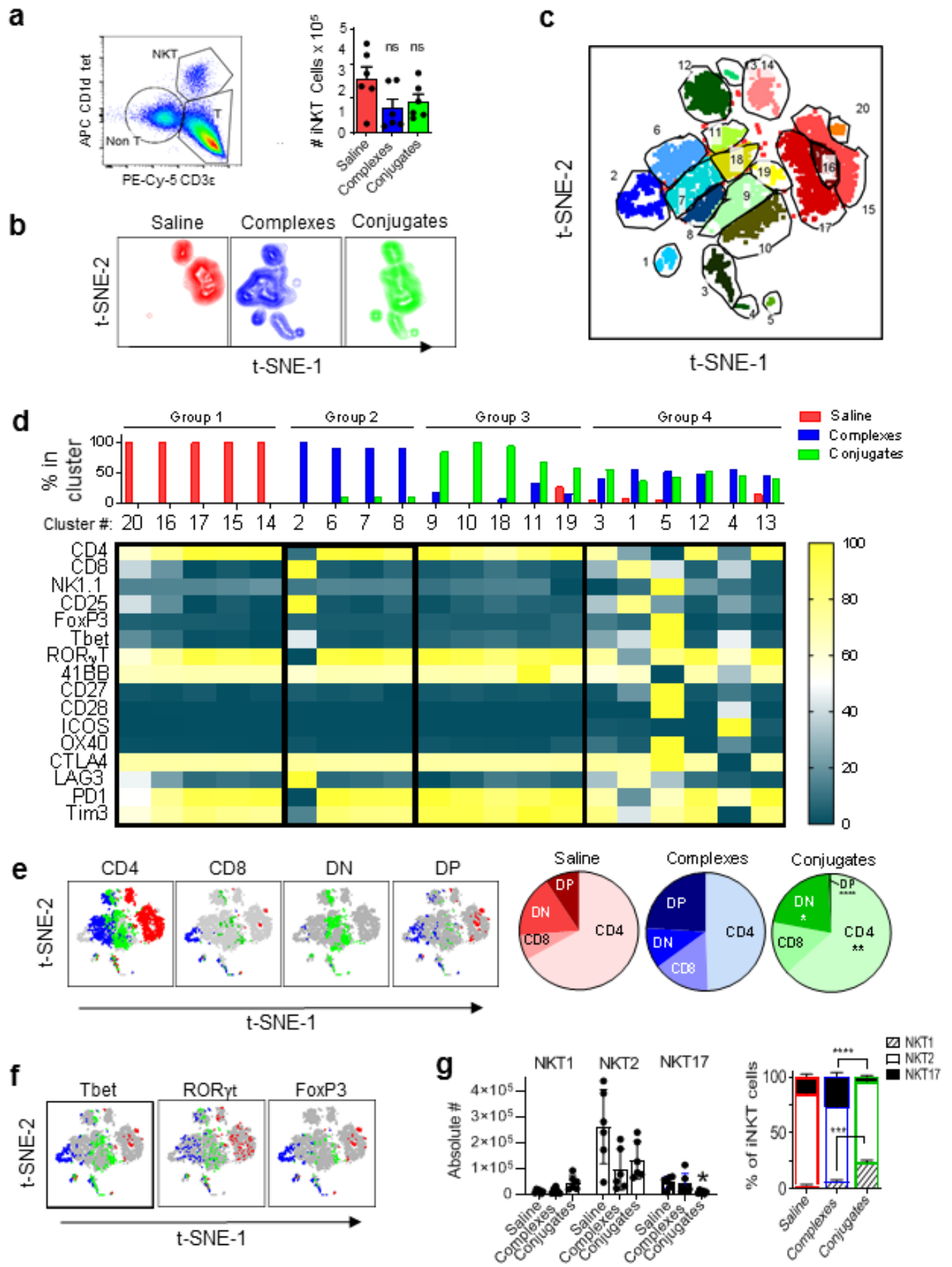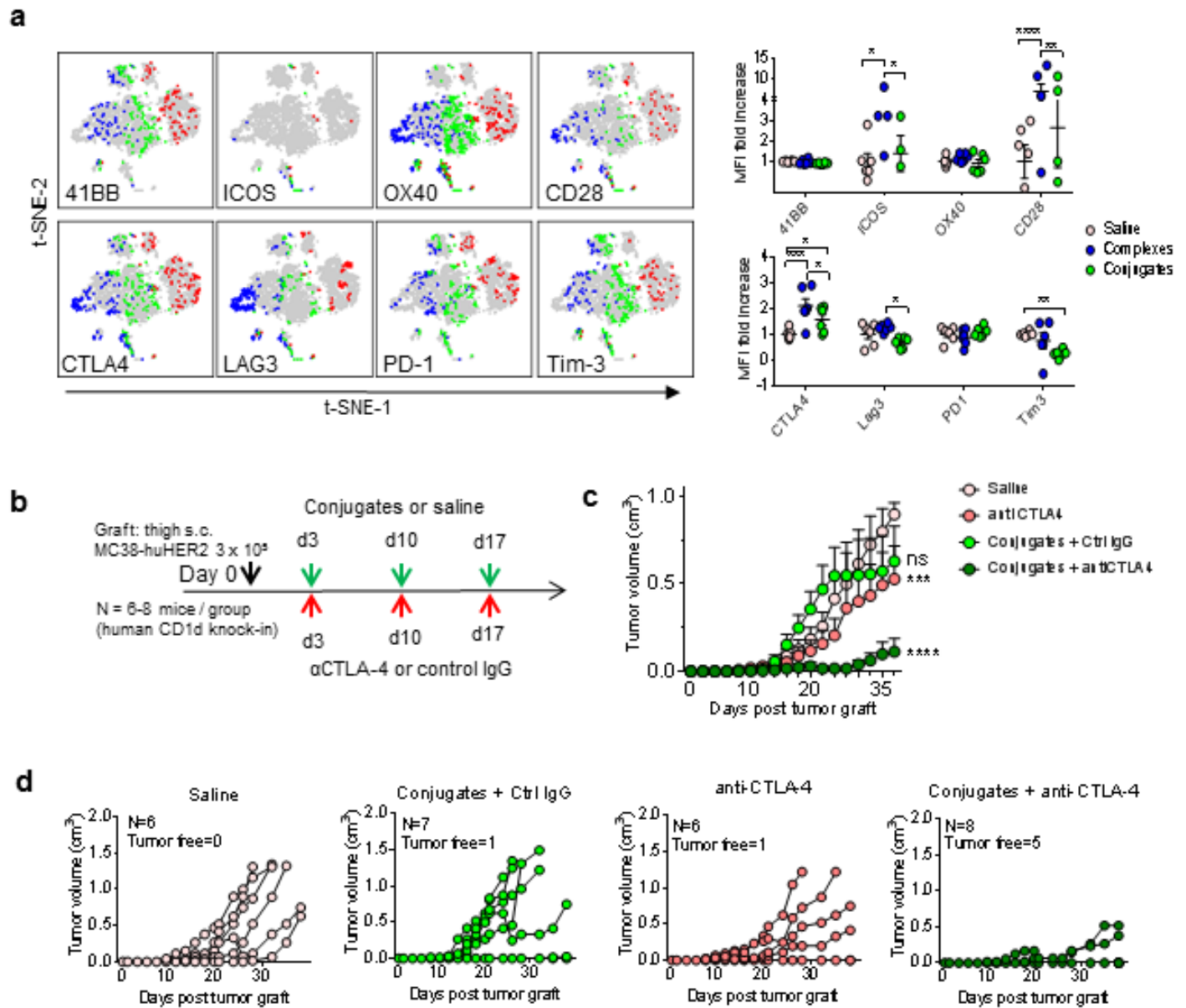Conjugates + anti-CTLA-4 — N=8, Tumor free=5

Supplemental Methods

Generation of noncovalent and covalent BiTEs

For glycolipid loading, glycolipids dissolved in aqueous buffer were added to fusion proteins at a molar ratio of 3:1 in PBS plus 0.05% Triton X-100 (for *in vitro* applications) or PBS + 0.05% Tween-20 (for *in vivo* experiments), and incubated for 16 hours at 22º C. For conjugate and conjugated BiTE formation, loaded complexes were transferred to ultra-low binding microtiter plate wells at 100 µl per well and cooled on ice. A fixed wavelength UV lamp (Schleicher & Schuell Rad-Free long wave UV lamp, λ = 365 nm) was placed directly over wells (mean distance to sample ~5 mm) containing complexes for 1 hour on ice to deliver a total dose of 600 mJoules/cm^2. Resulting conjugates and conjugated BiTEs were recovered from the wells, and excess glycolipid and detergent was removed using detergent-removal columns (Pierce) followed by buffer exchange into PBS using a 10 kDa MW cutoff centrifugal filtration unit (Amicon). Size exclusion chromatography using a S200 26/60 FPLC column (GE Healthcare) was performed to confirm the predominantly monomeric status of the conjugated BiTEs and remove trace amounts of multimers. All preparations of complexes and conjugates were confirmed to be free of significant levels of endotoxin (< 0.1 EU/mg) by Kinetic-QCL limulus amebocyte lysate test (Lonza).

Preparation of mouse splenocyte suspensions and TILs

Mouse spleens and tumors were harvested aseptically for preparation of single cell suspensions. Spleens were cut into fragments and gently ground between glass slides, and resulting suspensions were filtered through 40 µm nylon mesh, followed by

treatment with RBC lysis buffer (Sigma) for 3 minutes. The buffer was neutralized by adding 10 volumes of RPMI-1640 containing 10% FBS, centrifuged and resuspended in medium. Liver mononuclear cells were isolated from organs following treatment with Liberase (0.3 Wunsch units/ml) and 200 Units/ml DNase I (Roche) and passage through 40 μm nylon mesh, followed by Percoll gradient centrifugation as previously described (*45*). For isolation of tumor infiltrating lymphocytes (TILs), tumors were harvested from euthanized mice, cut into ~1 mm^3 pieces and processed using the enzyme solution provided in the Miltenyi mouse Tumor Dissociation Kit according to the supplier's instructions (Miltenyi Biotec). Cells were passed through a 40 μm nylon mesh, collected by centrifugation and resuspended 40% Percoll in RPMI-1640, and overlaid on 70% Percoll in RPMI-1640. This was centrifuged at 220 x g for 25 minutes at 15°C. The layer of lymphocytes from the interface of 40% and 70% Percoll was collected, treated with RBC lysis buffer, washed and resuspended in PBS with 5% FCS for antibody staining. For adoptive transfer studies and *in vitro* bioassays, iNKT cells were isolated from mouse splenocytes by immunomagnetic purification using the Miltenyi mouse NK1.1$^+$ iNKT purification kit according to the manufacturer's instructions (Miltenyi Biotec). Total T cells were isolated from spleens using Miltenyi mouse Pan-T cell isolation kit, and CD8 depletion was done using anti-CD8 beads (Miltenyi) for immunomagnetic negative selection. All magnetic bead purification steps were performed at 4° C.

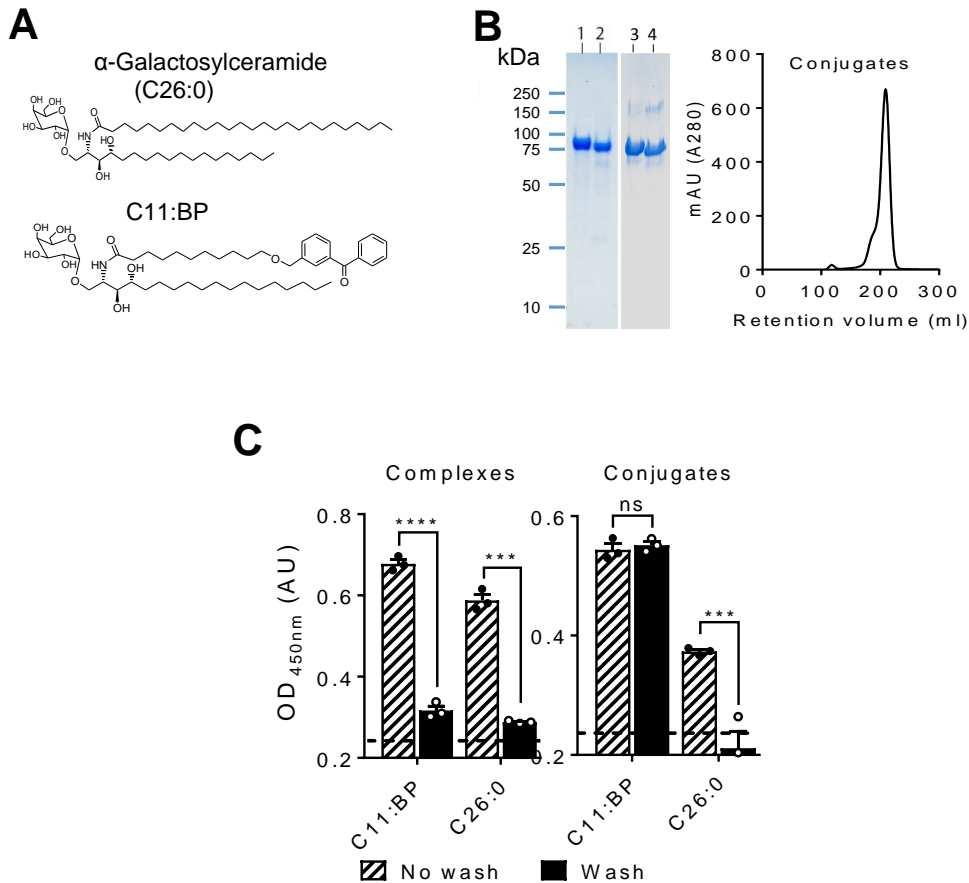**A**

α-Galactosylceramide
(C26:0)

C11:BP

B

C

Figure S1: Generation of covalent conjugates. A. Structures of glycolipid agonists. **B.** Coomassie blue stained SDS PAGE of purified fusion proteins (anti-human CEA-mCD1d-β2m and anti-huHER2-mCD1d-β2m (lanes 1 and 2), and anti-huHER2-hCD1d-β2m and control ScFv 1237-hCD1d-β2m (lanes 3 and 4)). Size exclusion chromatogram is shown of UV conjugated anti-humanHer2-mCD1d-β2m. **C.** ELISA showing covalent stabilization of conjugates formed between anti-huHER2-mCD1d-β2m fusion protein and C11:BP following photoactivation. Complexes (no UV exposure, left) or conjugates (UV treated, right) loaded with C11:BP or α-GalCer-C26:0 were incubated for 3 days with (black bars) or without (hatched bars) washing twice per day with PBS + 0.1% Triton X-100. Residual glycolipid bound to mCD1d was detected using biotinylated monoclonal antibody L363. Dashed line shows signal without glycolipid loading. ***P < 0.001, ****P < 0.0001, ns not significant; 2-way ANOVA with Sidak multiple comparison post test.
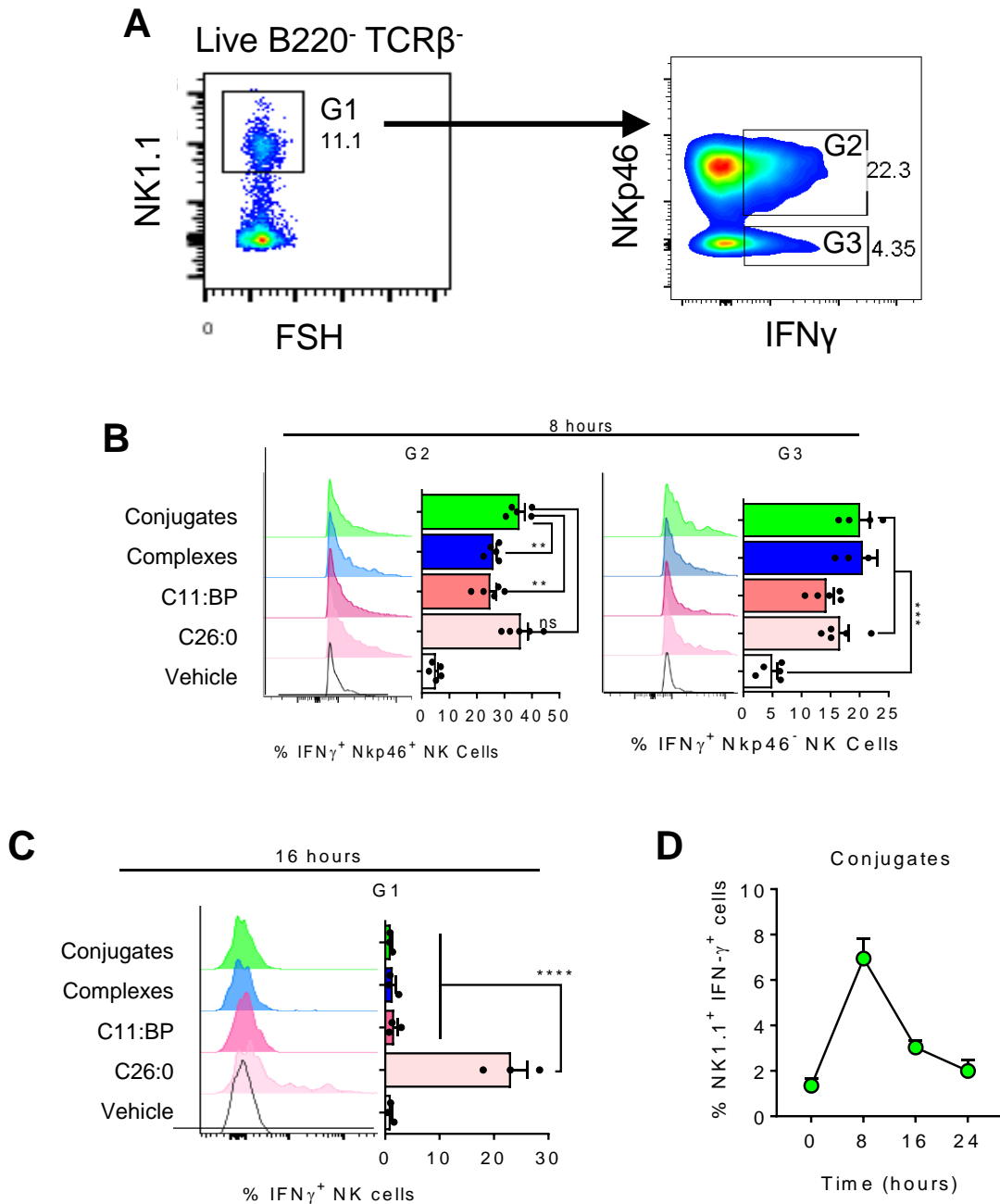
Figure S2: Conjugates cause transient but potent NK cell transactivation.
Transactivation of NK cells was determined by intracellular staining of NK cells for IFN-γ at 8 hours and 16 hours post stimulation with various adjuvants. **A.** Gating strategy for intracellular IFN-γ positive Nkp46 positive and Nkp46 negative NK cells from spleens at 8 hours. **B.** Representative histograms and bar graph for intracellular IFN-γ positive NKp46+ or Nkp46- NK cells purified at 8 hours (left panel) and incubated *in vitro* with brefeldin A for 4 hours prior to intracellular staining. **C.** similar analysis of total NK cells performed 16 hours after *in vivo* injections. **D.** Kinetics of NK transactivation with conjugate stimulation *in vivo.* **P < 0.01, ***P < 0.001, ****P < 0.0001, ns not significant; 2-way ANOVA and Sidak post-test for multiple comparisons.
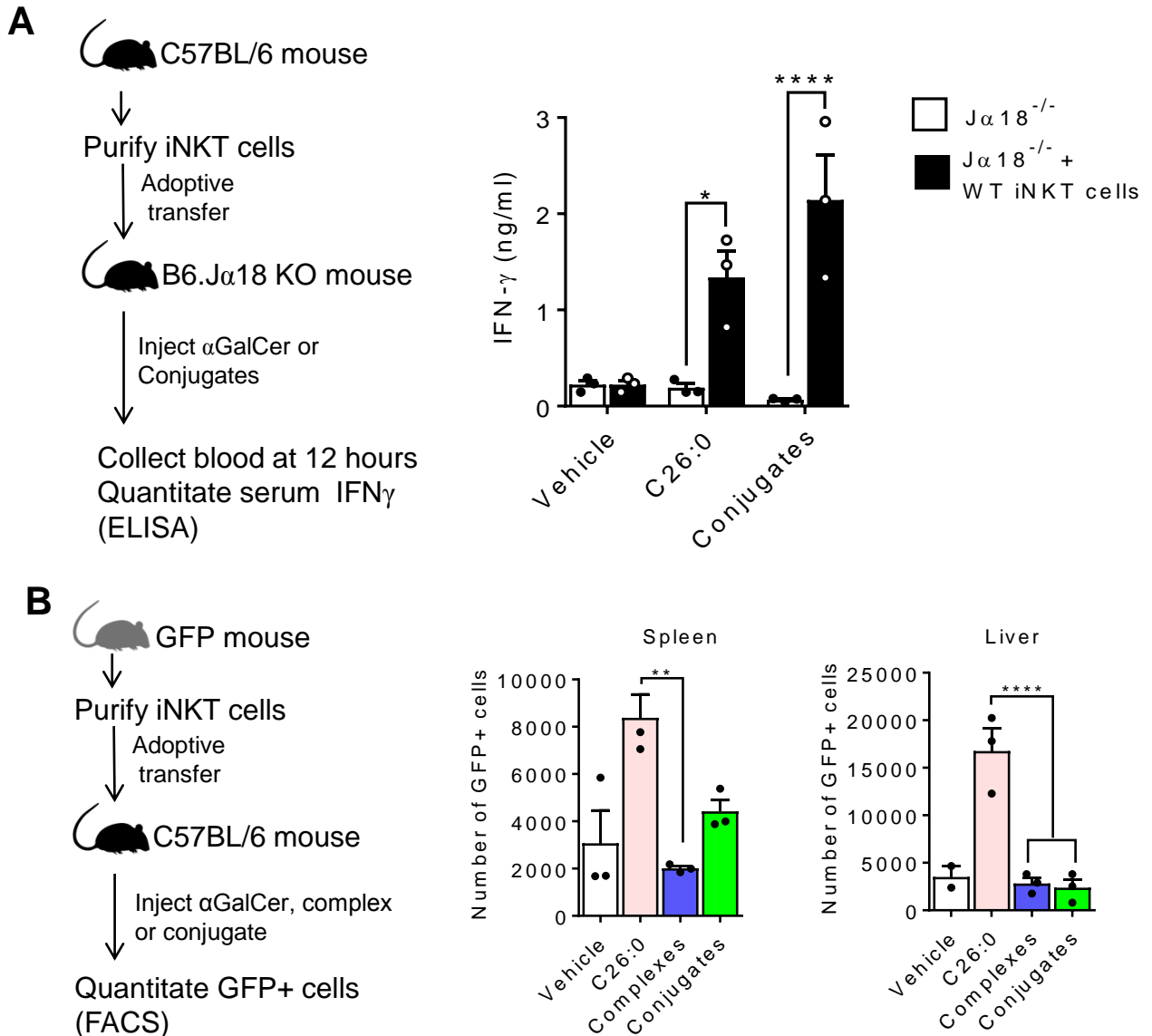
A

B

Figure S3: Responses to conjugates *in vivo*. A. Absence of responses in iNKT cell deficient mice and reconstitution by adoptive transfer of iNKT cells. Serum IFNγ was measured in Jα18-/- mice which lack iNKT cells 12 hours post injection with indicated stimuli. Mice were either unmanipulated (white bars) or recipients of 100,000 iNKT cells purified from livers of C57BL/6 mice and injected i.v. 16 hours prior to stimulation (solid bars). **B**. iNKT cells purified from livers of GFP transgenic mice were adoptively transferred into C57BL/6 mice. Mice were stimulated with free αGalCer C26:0 (0.4 nmol), complexes (100 µg) or conjugates (100 µg) 16 hours after the adoptive transfer. Spleen and liver were analyzed at 72 hours to quantitate GFP positive iNKT cells using FACS and green fluorescent beads to generate absolute cell counts. Data are means of triplicate samples ± 1SE. **P < 0.01; ****p<0.0001; two way ANOVA with Sidak test for multiple comparisons.

Figure S4: Specific binding of anti-HER2 conjugates to MC38-huHER2 cells and preferential retention in huHER2+ tumors. A. Expression of huHER2 and absence of endogenous CD1d or human CEA on MC38-huHER2 transfected cells was validated by flow cytometry. Light shaded histograms show specific staining for the indicated proteins, and dark histograms are isotype matched control antibody staining. **B**. APC-labeled tetramers of unloaded mCD1d or anti-HER2 mCD1d-ScFv were used to stain single cell suspensions from spleen, liver, kidney and MC38-HER2 cells to assess binding by FACS analysis. ****P < 0.0001, two way ANOVA with Sidak test for multiple comparisons. **C**. *In vivo* target specific cytotoxicity of conjugates was determined by mixing MC38 cells with MC38-huHER2 cells in various ratios before grafting on the thigh in mice. **D.** Direct visualization by click chemistry labeling of azido-modified C11:BP in tissue sections from MC38-huHER2 tumor bearing animals injected once with saline or anti-huHER2 conjugates. Scale bar 100 nm.

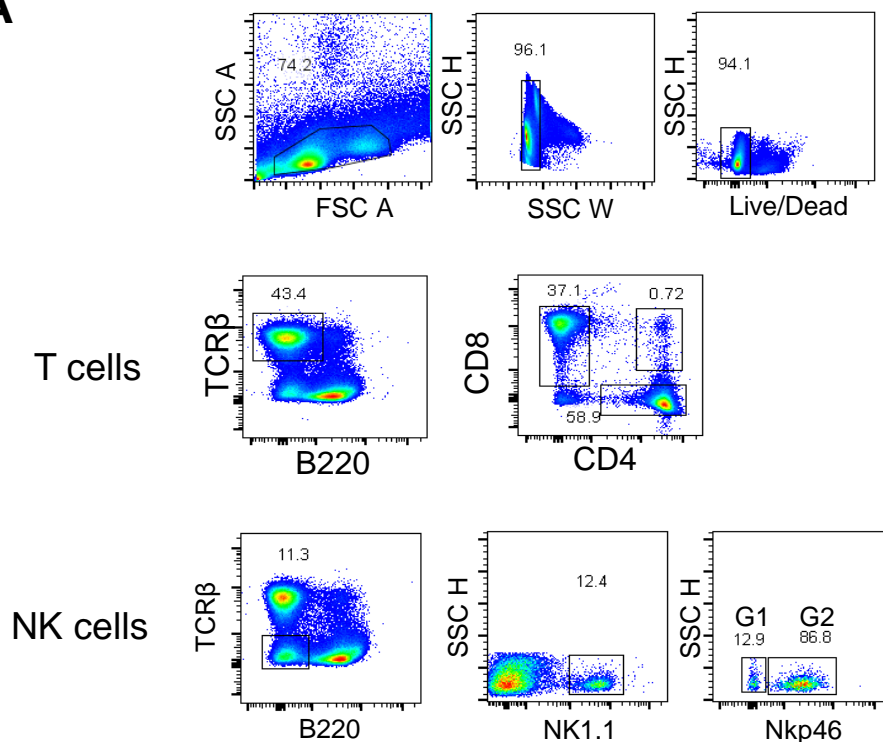**Figure S5: Gating for FACS analyses of TILs shown in Fig. 5. A.** Gates used for analyses of T cells and NK cells shown in Fig. 5C-F. **B.** Gates used for analyses of myeloid cells in Fig. 5G.

A.

C57BL/6 WT (N = 9 / group)

Graft: thigh s.c.
MC38-HER2
5×10^5

Day 0

Conjugates i.v.
d5   d12   d19

d5   d12   d19
αCTLA-4 i.p.

B.

Saline + Control IgG
Saline + aCTLA-4
Conjugate + Control Ig
Conjugate + aCTLA-4

ns
ns
***

C.

Saline+ Control Antibody
N=12
Tumor free=0

Saline+ anti-CTLA4
N=12
Tumor free=1

anti Her2 Conjugates +
Control Antibody
N=9
Tumor free=2

anti Her2 Conjugates +
anti CTLA4
N=9
Tumor free=5

Days post tumor graft

D.

Conjugates + anti-CTLA4
Conjugates + Control Ab
Saline + anti-CTLA4
Saline + Control Ab

Dead
Alive

Number of mice

Figure S6: Targeted conjugates and anti CTLA-4 synergize in C57BL/6 mice. A.
Scheme for combination treatment of MC38-huHER2 tumor bearing wild type C57BL/6
mice with conjugates plus anti-CTLA-4 blocking antibody. **B.** Tumor growth shown as
mean values for each treatment group (N = 9 mice per group). **C.** Tumor growth curves
for individual mice in each treatment group. The numbers of tumor free mice remaining at
the end of observation at day 55 are indicated. **D**. Summary of survival of mice at day 55.
***P < 0.001; ns, not significant; 2-way ANOVA with Sidak multiple comparison test.

Supplementary Table 1. Antibody conjugates and other reagents for flow cytometry

Marker (Specificity)	Fluorochrome/Tag	mAb Clone	Supplier (Cat. No.)	Resource Identifier	Dilution	Staining
mCD1d	FITC	1B1	BD Biosciences (561756)	RRID:AB_10894191	1:200	Surface
huHER2	Biotin	BAF1129	Biotechne	RRID:AB_355859	1:200	Surface
huCEA	FITC	Kat4c	Millipore (FCMAB204F)	RRID:AB_11213005	1:200	Surface
4-1BB	BV 650	1AH2	BD Biosciences (BDB740499)	RRID:AB_395075	1:250	Surface
B220	BV 750	RA3-6B2	BioLegend (103261)	RRID:AB_2734157	1:200	Surface
B220	PerCP-Cy5.5	RA3-6B2	Tonbo (65-0452-U100)	RRID:AB_26218921	1:200	Surface
B220	APC-Cy7	RA3-6B2	BD Biosciences (552094)	RRID:AB_394335	1:200	Surface
mCD1d tetramer	APC	NA	NIH Tetramer Core Facility	NA	7.5 µg/ml	Surface
CD3ε	PE-Cy5	145-2C11	BD Biosciences (553067)	RRID:AB_394599	1:200	Surface
CD4	PerCP	GK1.5	BioLegend (100432)	RRID:AB_893323	1:250	Surface
CD4	BV605	RM4-5	BD Biosciences (563151)	RRID:AB_2687549	1:250	Surface
CD8α	PB	53-6.7	BD Biosciences (558106)	RRID:AB_397029	1:200	Surface
CD8α	Alexa Fluor 700	53-6.7	eBiosciences (56-0081-82)	RRID:AB_494005	1:500	Surface
CD11b	Alexa Fluor 700	M1/70	BD Biosciences (557960)	RRID:AB_396960	1:250	Surface
CD11c	FITC	HL3	BD Biosciences (553801)	RRID:AB_395060	1:250	Surface
CD25	APC-Cy7	3C7	BioLegend (101918)	RRID:AB_2650982	1:250	Surface
CD27	PE/Dazzle 594	LG.3A10	BioLegend (124228)	RRID:AB_2565794	1:250	Surface
CD28	PE	JJ319	BD Biosciences (559984)	RRID:AB_397410	1:250	Surface
CD28	BV421	28.2	BD Biosciences (562613)	RRID:AB_2737676	1:200	Surface

Marker (Specificity)	Fluorochrome/Tag	mAb Clone	Supplier (Cat. No.)	Resource Identifier	Dilution	Staining
CD40L	BV480	Mr1	BD Biosciences (746825)	RRID:AB_2744077	1:250	Surface
CD45	PE-Cy7	30-F11	BioLegend (103114)	RRID:AB_312979	1:250	Surface
CD69	FITC	H1.2F3	BD Biosciences (553236)	RRID:AB_394725	1:250	Surface
CD80	PE	1G10	Novus-Bio (NBP1-28029)	RRID:AB_1852659	1:250	Surface
CD86	APC-Cy7	GL-1	BioLegend (105030)	RRID:AB_2244452	1:250	Surface
CTLA-4	AlexaFluor488	9D9	BioXcell	RRID:AB_10949608	1:250	Surface
F4/80	APC	BM8	BioLegend (123116)	RRID:AB_893481	1:250	Surface
FoxP3	eFluor450	FJK-16s	eBiosciences (48-5773-82)	RRID:AB_1518812	1:200	Intracellular
Gr-1 (Ly6-C, -G)	PerCP	RB6-8C5	BioLegend (108426)	RRID:AB_893557	1:250	Surface
ICOS	Brilliant Violet 510	C398.4A	BioLegend (313525)	RRID:AB_2562642	1:250	Surface
IFNγ	Alexa Fluor 700	XMG1.2	BD Biosciences (557998)	RRID:AB_396979	1:200	Intracellular
LAG3	PerCP-Cy5.5	C9B7W	BioLegend (125212)	RRID:AB_2561517	1:250	Surface
Live/Dead	DAPI	NA	Sigma (10236276001)	NA	1 µg/mL	Nuclear
Live/Dead	Fixable Blue	NA	ThermoFisher (L34955)	NA	1:500	Cytoplasmic
Live/Dead	Zombie NIR	NA	BioLegend (423106)	NA	1:1000	Cytoplasmic
NK1.1	BV421	PK136	BD Biosciences (562921)	RRID:AB_2728688	1:250	Surface
Nkp46	Alexa Fluor 700	29A1.4	BD Biosciences (561169)	RRID:AB_10561840	1:250	Surface
OX40	Brilliant Violet 605	OX-86	BioLegend (119419)	RRID:AB_2687175	1:250	Surface
PD-1	PerCP-eFluor 710	J43	eBiosciences (46-9985-82)	RRID:AB_11150055	1:200	Surface
PD-L1	PE	10F.9G2	BioLegend (124308)	RRID:AB_2073556	1:250	Surface
PD-L2	APC	B7-DC	ThermoFisher (17-5888-42)	RRID:AB_2573238	1:250	Surface

Marker (Specificity)	Fluorochrome/Tag	mAb Clone	Supplier (Cat. No.)	Resource Identifier	Dilution	Staining
RORγT	Brilliant Violet 786	Q31-378	BD Biosciences (564723)	RRID:AB_2738916	1:200	Intracellular
T-bet	Brilliant Violet 711	4B10	BioLegend (644820)	RRID:AB_2715766	1:200	Intracellular
TCRβ	PerCP-Cy5.5	H57-597	Tonbo (65-5961)	RRID:AB_2621911	1:200	Surface
Tim-3	Alexa Fluor 647	B8.2C12	BioLegend (134006)	RRID:AB_1626175	1:250	Surface

Supplemental Table 2. Mab and detection reagents used for ELISA analyses

MAb or reagent	Application	Species	Clone	Supplier (Cat. #)	Reagent Identifier	Working Dilution
Anti-IFNγ	Capture	Rat	R4-6A2	BD Biosciences (551216)	RRID:AB_394094	1:1000
Biotin anti-IFNγ	Detection	Rat	XMG1.2	BD Biosciences (554410)	RRID:AB_395374	1:500
Anti-IL4	Capture	Rat	11B11	BD Biosciences (554434)	RRID:AB_395390	1:500
Biotin anti-IL4	Detection	Rat	BVD6-24G2	BD Biosciences (554390)	RRID:AB_395362	1:500
Anti-IL12p70	Capture	Rat	9A5	BD Biosciences (554658)	RRID:AB_395493	1:500
Biotin anti-IL12p40/p70	Detection	Rat	C17.8	BD Biosciences (554476)	RRID:AB_395419	1:500
Streptavidin-HRP	Detection	*Strepto-myces avidinii*	na	BD Biosciences (554066)	RRID:AB_2868972	1:500